Elucidating the Role of Altered Heterogeneous Nuclear Ribonucleoprotein A1 Expression in the Pathogenesis of Neurodegeneration in an *In Vitro* Model of Multiple Sclerosis

A Thesis Submitted to the College of Graduate and Postdoctoral Studies in Partial Fulfillment of the Requirements for the Degree of Master of Science in the Department of Health Sciences

University of Saskatchewan

Saskatoon, Saskatchewan, Canada

Amber Anees

Permission to Use

In presenting this thesis in partial fulfillment of the requirements for a Postgraduate degree from the University of Saskatchewan, I agree that the Libraries of this University may make it freely available for inspection. I further agree that permission for copying of this thesis in any manner, in whole or in part, for scholarly purposes may be granted by the professor or professors who supervised my thesis work or, in their absence, by the Head of the Department or the Dean of the College in which my thesis work was done. It is understood that any copying or publication or use of this thesis or parts thereof for financial gain shall not be allowed without my written permission. It is also understood that due recognition shall be given to me and to the University of Saskatchewan in any scholarly use which may be made of any material in my thesis.

Requests for permission to copy or to make other use of material in this thesis in whole or part should be addressed to:

Head of the Department of Health Sciences
University of Saskatchewan
2D01 Health Sciences Building, 107 Wiggins Road
Saskatoon, Saskatchewan S7N 5E5 Canada

College of Graduate and Postdoctoral Studies
University of Saskatchewan
116 Thorvaldson Building, 110 Science Place
Saskatoon, Saskatchewan S7N 5C9 Canada

Abstract

Neuronal and axonal damage, collectively known as neurodegeneration, are salient pathogenic features of multiple sclerosis (MS) and are thought to underlie permanent disability in MS, particularly in progressive forms of the disease. Despite decades of research, the etiology of neurodegeneration in MS remains relatively unknown and there are no treatments available that target its pathogenesis. Research in MS as well as other neurologic diseases has established that dysfunctional RNA binding proteins (RBPs) are a prominent pathogenic feature and may contribute to the pathogenesis of neurodegeneration. Neurons from MS cortex have been shown to exhibit dysfunctional features of the RBP heterogeneous nuclear ribonucleoprotein A1 (hnRNP A1), whereby hnRNP A1 is mislocalized from its homeostatic nuclear location to the cytoplasm, resulting in loss of hnRNP A1 function within the neuron.

We hypothesized that loss-of-function of hnRNP A1 modelled using siRNA in differentiated Neuro-2a cells would have detrimental effects on neuronal health and viability. Through RNA sequencing (RNAseq) followed by gene ontology (GO) analyses, we found that hnRNP A1 is involved in important biological processes, including RNA metabolism, neuronal function, neuronal morphology, neuronal viability, and stress granule (SG) formation. We confirmed several of these roles by showing that hnRNP A1 knockdown caused a reduction of neurite outgrowth ($p<0.001$), which correlated with decreased hnRNP A1 expression ($p<0.05$), increased cell cytotoxicity ($p<0.05$), and increased punctate staining of a necroptotic cell death marker, phospho-mixed lineage kinase domain like pseudokinase (pMLKL). Additionally, we demonstrated that hnRNP A1 knockdown disrupts the formation of cytoplasmic SGs ($p<0.0001$) after stress induction.

These findings present novel insights into how hnRNP A1 loss-of-function in neurons may contribute to neuronal dysfunction and death. Further, it implicates hnRNP A1 dysfunction, particularly decreased hnRNP A1 expression, in the pathogenesis of neurodegeneration in MS and other neurodegenerative diseases.

Acknowledgement

Foremost, I would like to extend my sincere gratitude to my supervisor, Dr. Michael Levin, who took me on as a master's student and offered me continuous support and guidance in both my research and educational pursuits. I am greatly appreciative for his patience and ongoing advice over the course of my graduate degree. I would also like to express my deepest thanks and appreciation to Dr. Hannah Salapa, who has been an incredible mentor and teacher. Thank you for all that you have taught me; this project could not have been completed without your guidance and support. Thank you to my wonderful committee members: Dr. Francisco Cayabyab and Dr. Anand Krishnan for all their insight and valuable feedback.

Thank you to all the wonderful people at the CMSNRC and special thanks to Shannon Berko for always being the joy of the lab and bringing a smile to everyone's faces. Thanks to the lifelong friends I made at the lab; Nataliya Tokarska and Muxue Li, who were incredibly supportive and never let a single day go by without a laugh. I will forever value our friendship.

Extra special thanks to my loving significant other, Mr.USA, your endless support for all my passions and endeavors means the world to me. Thank you for all that you have taught me and for showing me how beautiful life is.

Lastly, I would like to thank my ever so supportive and loving family. Without whom nothing would have been possible, and I am extremely blessed and grateful for all that you have taught me and the wisdom you have bestowed upon me. Alhamdulillah.

Table of Contents

List of Tables

List of Figures

Abbreviations

AD	Alzheimer's disease
ALS	Amyotrophic later sclerosis
BDNF	Brain derived neurotrophic factor
BMP4	Bone morphogenetic protein 4
cAMP	cyclic AMP
CNS	Central nervous system
CSF	Cerebral spinal fluid
CypB	Cyclophilin B
CyPD	Cyclophilin D
ddH_2O	Double-distilled water
DE	Differentially expressed
DMEM	Dulbecco's modified eagle's medium
dsRBMs	Double-stranded RNA binding domains
EAE	Experimental autoimmune encephalomyelitis
ECL	Enhanced chemiluminescence
EGFR	Epidermal growth factor receptor
eIF2α	Eukaryotic initiation factor 2 α
eIF4A	Eukaryotic initiation factor 4A
FBS	Fetal bovine serum
FTLD	Frontotemporal lobar dementia
FUS/TLS	Fused in Sarcoma/ Translocated on Liposarcoma
G3BP1	GTPase-activating protein SH3-domain protein 1
GO	Gene ontology
GWAS	Genome wide association studies
HAM/TSP	HTL V-1 associated myelopathy/ tropical spastic paraparesis
HIV-Tat	HIV-1 trans activator of transcription
hnRNP A1	Heterogeneous nuclear ribonucleoprotein A1
hnRNPs	Heterogenous nuclear ribonucleoproteins
lκBα	Inhibitory subunit of the nuclear factor κB
INF- gamma	Interferon γ

MBP	Myelin basic protein
MLKL	Mixed lineage kinase domain like pseudokinase
MOG	Myelin oligodendrocyte glycoprotein
MRI	Magnetic resonance imaging
MS	Multiple sclerosis
NAWM	Normal appearing white matter
NF-κB	Nuclear factor κB
NF-L	Neurofilament light
NGF	Nerve growth factor
NOVA1	Neuro-oncological ventral antigen 1
PBS	Phosphate buffered saline
PBS-T	Phosphate buffered saline + Triton-X 100
PCA	Principal component analysis
PD	Parkinson’s’ disease
PLP	Proteolipid protein
pMLKL	Phospho- mixed lineage kinase domain like pseudokinase
PPMS	Primary progressive multiple sclerosis
PTBP1	Polypyrimidine tract-binding protein
RA	Retinoic acid
RBFOX1	RNA binding protein, fox-1 homolog
RBPs	RNA binding protein
RIPK1	Receptor Interacting Serine/Threonine Kinase 1
RIPK3	Receptor Interacting Serine/Threonine Kinase 3
RNAseq	RNA sequencing
RNP	Ribonucleoprotein
RNS	Reactive nitrogen species
ROS	Reactive oxygen species
RRMS	Relapsing remitting multiple sclerosis
SGs	Stress granules
SMA	Spinal Muscular Atrophy
SMN	Survival of motor neuron

SPMS	Secondary progressive multiple sclerosis
TBST	TBS + 0.1% Tween-20
TDP-43	TAR DNA binding proteins 43kDa
TGFβ1	Transforming growth β 1
TIA-1	T-cell-restricted intracellular antigen-1
TNF alpha	Tumor necrosis factor α

Parts of this thesis are adapted from Anees et al. 2021[1]. AA designed and performed the research, analyzed the data, and wrote the paper in collaboration with other authors under the supervision of MCL.

CHAPTER 1: INTRODUCTION

1.1 Multiple Sclerosis

1.1.1 History of Multiple Sclerosis and subtypes

Multiple Sclerosis (MS) is a chronic, debilitating disease of the central nervous system (CNS) primarily characterized by autoimmune-mediated destruction of myelin as well as loss of or damage to neurons and axons, known as neurodegeneration. Affecting over 2 million individuals worldwide, MS remains one of the most prevalent neurologic diseases among young adults. Onset of disease predominantly occurs between the ages of 20 and 40 and women are disproportionately affected at a three to one ratio[2].

Over a century has passed since Jean-Martin Charcot, a neurologist at the Hopital de Salpetriere in Paris, France, established MS as a distinct disease and described its pathogenesis as a dissemination of plaque-like sclerosis[3]. Following advancements in histological staining in the 20th century, Dawson, J.W. (1916)[4] gave insights into the inflammatory milieu and myelin damage that take place in MS. With the advent of modern technology such as magnetic resonance imaging (MRI), visualization of MS plaques and lesions in live patients was revolutionized. This allowed pathological changes, such as focal lesions, to become apparent in regions of the white matter, grey matter, brain stem, spinal cord and optic nerve throughout the course of the disease[5]. It is now understood that these plaques are the central areas where inflammatory infiltration, demyelination, cell death, gliosis and neurodegeneration take place.

The pathogenesis of MS is complex, and its etiology remains incompletely understood, however several efforts have been made to characterize the disease course into distinct clinical phenotypes. The signs and symptoms of MS are heterogeneous amongst patients and include, but are not limited to, numbness or weakness in one or

more limbs, partial or complete loss of vision, unsteady gait, and fatigue. These variety of clinical symptoms correlate with the distinct spatiotemporal lesions located within the CNS. Most MS patients are diagnosed with relapsing-remitting MS (RRMS), which is characterized by clinical episodes of partially or fully reversible neurologic exacerbations, otherwise known as relapses, and these can last up to several weeks and are usually followed by periods of stability where the disease state appears latent[5]. The International Panel of the Diagnosis of MS, defines these exacerbations as "patient-reported symptoms or objectively observed signs typical of an acute inflammatory demyelinating event" within the diagnosis criteria, usually referred to as "MacDonald criteria'[6,7]. A subset of patients with RRMS eventually transition into a more progressive phase of disease known as secondary progressive MS (SPMS) where there is an accumulation of disability that correlates with neurodegeneration[8], with rare instances of stability[9–11]. The more challenging to treat and far less understood clinical subtype is primary progressive MS (PPMS), in which patients experience continual progressive neurologic dysfunction from disease onset with no signs of remission or stability.

1.1.2 Pathogenesis and immunopathology of Multiple Sclerosis

In general, it is believed that the pathogenesis of MS initiates from the compromised integrity of the blood-brain barrier, which results in peripheral immune infiltration of autoreactive lymphocytes into the CNS. The ensuing consequences are multifarious, for example, evidence of demyelination is a prominent feature of disease and activated macrophages laden with myelin debris have been found early on in MS lesions[12]. Inflammatory infiltrates can also directly attack axons of neurons resulting in axonal transection and neuronal dysfunction[13], all while activated microglia augment the inflammation and also attempt to salvage the integrity of neurons by remyelinating. If remyelination fails, the outcome is chronic neurodegeneration and degenerating axons. In addition to this milieu of tissue injury, reactive astrocytes can cause gliosis, which may serve as a significant barrier for repair[12].

The clinical phenotypes in MS exhibit distinct pathological hallmarks. For example, in patients with RRMS, neuropathological and MRI data suggests that ongoing inflammation and the formation of new white matter lesions are prominent features[11,14].

These inflammatory areas are generally occupied by T-cells, B-cells, activated macrophages and microglia[9,11]. Lesions can also result in the local production of pro-inflammatory cytokines and chemokines, altogether contributing to the complete demyelination, which is often accompanied by a degree of axonal damage[11,15].

In comparison, progressive disease courses exhibit rare instances of new demyelinating lesions in the white matter and are instead disseminated with cortical demyelination and diffuse atrophy in areas of the grey matter, white matter and so called normal appearing white matter (NAWM)[11,16]. Pathological analyses of patients with progressive MS have also shown intense signs of microglial activation and the formation of microglial nodules in the NAWM[17].

While many have alluded to focal inflammation and then subsequent accumulation of inflammation as being the main culprits of injury seen throughout the whole brain, there have been progressive disease cases demonstrating that there is NAWM injury without a preceding inflammatory phase. Although post inflammatory neurodegeneration is a prominent feature in MS, it is now understood that neuronal and axonal damage seen in MS may at least partly be independent from the inflammatory storm. This has been underscored by the observation that treatment with immunomodulatory drugs that sufficiently modulate peripheral inflammation and demyelination, have been insufficient to inhibit neuronal loss, especially in progressive disease[18].

1.1.3 Neuronal and axonal damage

The importance of neuronal and axonal damage in MS is highlighted by robust studies showing that severity of disease correlates with the degree of axonal injury[13,19–22]. Early investigations into axonal damage revealed that significant axonal damage occurs during the active demyelination stage in new lesions and that axonal injury is related to the degree of macrophage infiltration within those lesions[13,23]. This supported the hypothesis that toxic inflammatory mediators were involved in axonal damage during active demyelination. However, it is now understood that neuronal and axonal damage is at least partially independent from the inflammatory and demyelination processes. For example, inactive plaques, which are characterized by little to no inflammation, demonstrate slow smoldering axonal degeneration[24]. It is believed that this type of

continuous low grade axonal damage may persist for years and account for a greater global loss of axons in MS than axonal degeneration in active plaques. Further, this may also account for the gradual progression of clinical impairment seen in progressive disease.

1.1.4 Cell death in Multiple sclerosis

Cellular death of neurons and oligodendrocytes has been shown to contribute to the pathogenesis of MS. The predominant mechanism of cell death in MS remains elusive, however there are several hypotheses that have alluded to the involvement of regulated cell death mechanisms such as apoptosis, and more recently, necroptosis.

The involvement of apoptotic cell death in MS was among the early hypotheses examined. Apoptosis encompasses both intrinsic and extrinsic pathways, both of which are tightly regulated and result in distinct morphological changes regulated by a set of caspases called the initiator and effector caspases. Initiator caspases, namely caspase-2, -8, -9 and -10 are responsible for the activation of the caspase cascade in apoptosis[25]. The effector caspases are caspase-3, -6 and -7 and are responsible for the execution of apoptotic cell death and dismantling of targeted cellular proteins[25]. Apoptosis in resident CNS cells is believed to be initiated by inflammation in MS[26]. For example, tumor necrosis factor-alpha (TNFα) and interferon-gamma (INFγ) produced by infiltrating T-cells, macrophages and activated microglia are capable of inducing apoptosis in oligodendrocytes[27]. This was further underscored by studies in experimental autoimmune encephalomyelitis (EAE), an animal model of MS, where it was observed that mice that expressed the caspase inhibitor, p35, in their oligodendrocytes were resistant to the development of EAE[27]. Further, it has been shown that neurons exposed to cerebrospinal fluid (CSF) from MS patients undergo apoptosis through increased caspase-3 activity, suggesting an important role for apoptosis in mediating neuronal cell death in MS.

More recently, necroptosis has been shown to have a prominent role in the death of both oligodendrocytes and neurons in MS[28,29]. Induction of necroptosis requires both the inactivation of caspase-8, an initiator of apoptosis, as well as the sequential activation of Receptor Interacting Serine/Threonine Kinase 1 (RIPK1), Receptor Interacting Serine/Threonine Kinase 3 (RIPK3) and subsequent phosphorylation of mixed lineage

kinase domain like pseudokinase (MLKL). Necroptosis activation culminates in the formation of protein oligomers called necrosomes, consisting of RIPK1, RIPK3 and phospho-MLKL (pMLKL), which penetrate the cell membrane leading to cell death. Studies examining cortical grey matter lesions in MS have revealed evidence of defective caspase-8 activation, accompanied by increased activation of RIPK1, RIPK3 and MLKL, suggesting the involvement of necroptosis[28,29]. Furthermore, one study showed that oligodendrocyte death in the cuprizone animal model of MS was primarily mediated through necroptosis and that TNFα treatment was sufficient to induce necroptotic death in oligodendrocytes *in vitro*[29]. An additional study observed that there was a significant increase in activated necroptotic proteins in MS neurons from post-mortem brains as compared to healthy controls[28]. Strikingly, they showed that the density of neurons with pMLKL inversely correlated with the age at progression, disease duration and age at death, underpinning the important involvement of necroptosis in mediated cell death in MS.

1.2 Neurodegeneration in Multiple Sclerosis

1.2.1 Mechanisms of neurodegeneration

Understanding the molecular mechanisms of neuronal and axonal damage is an ongoing pursuit in MS research. Currently, no treatments exist that have been able to successfully alter the course of neurodegeneration in MS. Several hypotheses exist to explain the driving force behind neurodegeneration, including mitochondrial injury, deficits in axonal transport, and immunological mechanisms.

Our current insight into neurodegeneration in MS largely comes from the EAE animal model of MS, which exhibits many of the neuropathological features of MS, including neuron loss and axonal damage[30,31]. These studies were the first to demonstrate the contribution of oxidative stress to neurodegeneration[31]. Further insight from EAE and MS lesions revealed abundant production of reactive oxygen species (ROS) and reactive nitrogen species (RNS) by microglia and macrophages[31–33]. The deleterious effects of these neurotoxic molecules were demonstrated in an *in vivo* study showing that the application of nitrogen and oxygen donors, which are required for ROS and RNS generation, to the spinal cords of healthy mice resulted in EAE-like axonal

degeneration in the absence of demyelination[31]. Increased levels of ROS and RNS can also increase the risk of mitochondrial damage, which has previously been hypothesized to be a cause of tissue injury in MS[34]. Considering the elemental role of mitochondria in energy production and basic metabolic functioning within a neuron, their dysfunction can be foreseen to cause detrimental effects. Although ROS production and mitochondrial deficiencies usually increase with age, one study showed that SPMS patients exhibited increased levels of deletions in their mitochondrial DNA as compared to both RRMS patients and age-matched controls[35]. Additionally, mitochondrial damage can be triggered by the mitochondrial permeability transition pore (MPTP), which is regulated by the matrix protein, cyclophilin D (CyPD)[36]. The MPTP plays a vital role in cell death as its opening allows the influx of non-specific intermembrane proteins into the cytosol and subsequent rupture of the outer membrane of the mitochondria[37]. Mice that are deficient in CyPD have been shown to develop a milder EAE disease course accompanied by decreased levels of axonal damage[36]. These studies support the idea that mitochondrial damage and dysfunction may contribute to neurodegeneration in progressive disease.

Another hypothesized mechanism of neuronal and axonal damage in MS is dysfunctional axonal transport, which has been previously implicated in many other neurodegenerative diseases[38]. Proper axonal transport is an essential part of neuronal health, and is primarily carried out by two major microtubule motors called kinesins, involved in anterograde transport, and dyneins, involved in retrograde transport[39]. The association between dysfunctional axonal motor proteins and MS susceptibility was first delineated through genome wide association studies (GWAS)[40] and has now been supported by many neuropathological studies showing hallmarks of inadequate axonal transport[41,42]. For example, examination of MS white matter revealed reduced abundance of the motor protein KIF5A, a kinesin, along with its associated cargo. Reduced abundance of motor proteins and the resultant dysfunction are hypothesized to result in discernible amounts of protein and organelle aggregates, which are commonly observed in MS tissue[42].

Lastly, the contribution of chronic inflammation has been a long-standing hypothesis in mechanisms contributing to neurodegeneration (Figure 1.1). Examination

of progressive cortical grey matter pathology revealed a positive correlation between diffuse inflammatory infiltrates and neurodegeneration[18,43]. There is substantial evidence that shows that T- cell effector subsets and cytokines such as IL-1 have the ability to directly cause neuronal and axonal damage in EAE and MS[44,45]. For example, Siffrin et al.[46] demonstrated that the interaction between myelin oligodendrocyte glycoprotein (MOG) specific Th17 cells and neuronal cells has the ability to cause a considerable amount of axonal damage. Further, it was suggested that Th17 cells likely perturb neuronal calcium levels leading to large scale neuronal dysfunction[46].

B-cells have also been implicated in driving inflammatory events that lead to neurodegeneration, especially in progressive disease. B-cells are involved in a myriad of functions such as antibody production, antigen presentation, enhanced excretion of pro-inflammatory cytokines and altering production of regulatory cytokines, which may impact complement activation and T-cell function[47,48]. Studies have established the presence of autoantibodies to myelin antigens such as proteolipid protein (PLP), myelin basic protein (MBP) and MOG, which have been shown to play a key role in demyelination via complement cascade activation[9,49–51]. However, recent studies have also indicated that autoantibodies to non-myelin antigens such as potassium channels, neurofilaments, neurofascin and RNA binding proteins (RBPs) are crucial mediators of neurodegeneration[52–56]. For example, research by Huizinga et al.[52] has shown that autoimmunity to the neuronal cytoskeletal protein neurofilament light (NF-L) is sufficient to induce axonal damage and spasticity, a common feature of MS. Another study showed that intrathecal production of anti-NF-L autoantibodies were significantly higher in patients with SPMS and PPMS as compared to age-matched controls[57]. Similarly, RBPs are another prime example of how autoimmunity can cause neuronal damage, for example, autoantibodies to the RBP known as heterogenous nuclear ribonucleoprotein A1 (hnRNP A1) have been implicated in the pathogenesis of neurodegeneration in MS[54–56].

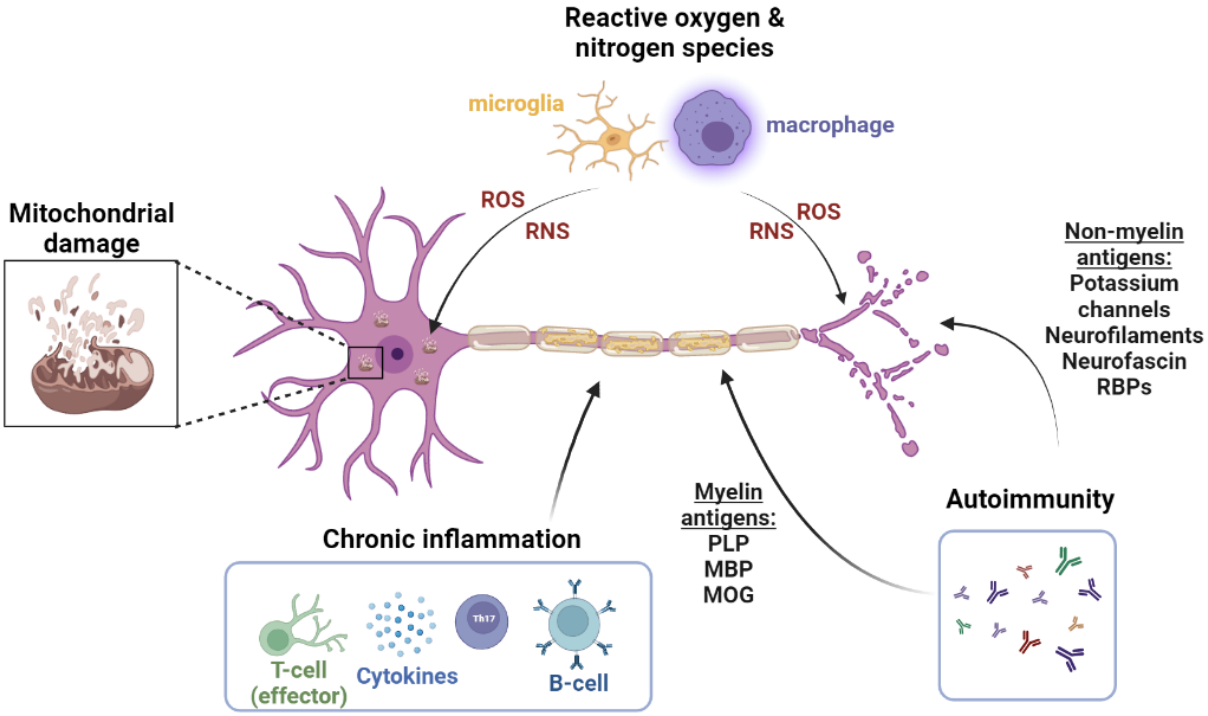

Figure 1.1 Schematic of mediators of neuroaxonal damage. Several hypotheses explain how neurodegeneration culminates in MS. Mitochondrial damage can be triggered from the MPTP resulting in rupture of mitochondrial membrane. Reactive oxygen and nitrogen species released from microglia and macrophages cause mitochondrial dysfunction and axonal degeneration. Autoimmunity to both myelin antigens such as PLP, MBP and MOG, as well as non-myelin antigens such as potassium channels, neurofilaments, neurofascin and RBPs can contribute to neurodegeneration. Lastly, chronic inflammation mediated by T-cell effector subsets, influx of cytotoxic cytokines, Th17 cells and B-cells are thought to cause neuronal cell damage.

1.3 RNA metabolism

1.3.1 RNA binding proteins

RBPs are dynamic proteins, which bind RNA via modular RNA binding domains and, as a result, change the destiny and function of the bound RNA. Although there are several hundred known RBPs, some common structural features of the RNA binding domains of RBPs consist of RNA-recognition motifs, zinc finger domains, K homology

domains and double-stranded RNA binding domains (dsRBMs)[58]. As a result, RBPs are known to play an integral role in many aspects of RNA metabolism, some of which include mRNA maturation, translation, processing as well as regulating the stability of cytoplasmic and nuclear stress granules (SGs)[59,60].

In neurons, precise regulation of protein homeostasis is required to maintain the highly polarized state, in which RBPs are heavily involved[61]. Several studies have alluded to the existence of neuron specific RBPs that partake in important steps of pre-mRNA maturation. Some examples include the polypyrimidine tract-binding protein (PTBP1), neuro-oncological ventral antigen 1 (NOVA1) and RBP, fox-1 homolog (RBFOX1), all of which are involved in neuron-specific RNA splicing events[62–64]. More specifically, RBPs have the ability to fine tune alternative splicing events in response to any neuronal cell signal and can alter the course of neuronal differentiation[64,65]. The ability of RBPs to tightly regulate gene expression is also accomplished through their ability to positively interact with other RBPs through collaborative binding[66]. While RBPs have distinct specialized functions, RBP families are also known to be quite versatile and possess some redundant functions for instances when another vital RBP loses its proper functioning.

1.3.2 RNA granules

RBPs are also involved in the formation of membraneless organelles known as ribonucleoprotein (RNP) granules. Multiple types of RNA granules have been identified that are specific to the cell type, cellular compartment, and function they perform. Examples of RNA granules include germ granules, Cajal bodies, processing (P)-bodies and SGs. Germ granules, for instance, are specific to germ cells and are foci of translationally repressed RNA that form in the cytoplasm[67]. Cajal bodies are specific to neurons, even though they can be found in embryonic and tumor cells, and are known to form RNA foci within the nuclei of those cells[68]. P-bodies and SGs are RNP granules, which assemble in the cytoplasm of cells. P-bodies are primarily composed of mRNA not engaged in translation that are being processed for degradation, while SGs are foci of mRNA that assemble around translational machinery in response to a cell stressor[69].

It is now understood that formation of these RNP granules is driven through liquid-liquid phase separation, a reversible biological process by which like particles form

condensate droplets within the cell[70]. The cores of these condensates are composed of RBPs with highly disordered regions known as prion like domains, which interact with RNAs and RNA binding domains of RBPs, together forming aggregates through phase separation[71]. In pathologic cases such as in neurodegenerative diseases, the prion like domains of RBPs alter the course of the liquid condensates to form stable aggregates within the cytoplasm. For example, RBPs like TAR DNA binding protein 43kDa (TDP-43), Fused in Sarcoma/ Translocated on Liposarcoma (FUS/TLS), and hnRNP A1 have all been shown to be part of pathological inclusions within the cytoplasm of neurons in neurodegenerative diseases[72–74]. Further insight has revealed that these inclusions are primarily driven through disease causing mutations within the prion like domains of these RBPs, ultimately resulting in altered protein localization, including mislocalization from their homeostatic nuclear location to the cytoplasm[75,76]. This has led many to query whether there is a loss of RBP function or a cytoplasmic gain of toxicity in neurons, which could lead to cellular dysfunction.

1.3.3 Dysfunctional RNA binding proteins

Dysfunction of RBPs, referred to as “RNA binding proteinopathies” has been recently established as a contributing factor to neuronal pathology in neurodegenerative disease, leading to wide scale disturbances in RNA processing and activity[77–79]. The leading causes of these proteinopathies are (1) disease causing mutations, (2) entrapment of RBPs within large protein aggregates as a result of other mutant proteins and (3) autoantibodies to certain RBPs[59]. This is especially evident in neurodegenerative diseases such as amyotrophic lateral sclerosis (ALS) and frontotemporal lobar dementia (FTLD) and most recently MS, where the combination of mutations and autoantibodies to RBPs results in a multitude of pathological consequences[54,60,75,80]. Consequences of RBP dysfunction most commonly include mislocalization from the nucleus to the cytoplasm, disruption of RNA metabolism and formation of cytoplasmic SGs[78,81,82] (Figure 1.2).

For example, mutations in the gene encoding for TDP-43 have been found in patients with ALS[83] and additional *in vivo* studies have shown that these mutant forms result in developmental delays and neural apoptosis[84]. Additional insight demonstrates that mislocalization, cytoplasmic accumulation and ubiquitination of TDP-43 are primitive

signs of insoluble aggregate formation within motor neurons in ALS patients, which can be toxic to cells[85]. Similarly, mutations within FUS/TLS have been identified in patients of ALS, leading to the formation of cytoplasmic aggregates and widescale disruptions in RNA processing[86,87]. FUS/TLS cytoplasmic aggregates have also been shown to contribute to neuronal degeneration in an ALS mouse model[88]. These examples emphasize the idea that RBP aggregation in the cytoplasm may directly cause cell toxicity through interfering with the proteostatic network within the cytoplasm.

Another leading hypothesis of RBP dysfunction is that widescale disruptions in RNA metabolism is due to a loss of functionality of RBPs in neurodegenerative diseases. This is supported by observations of nuclear clearance of TDP-43 in ALS patients and relevant animal models, which has been shown to induce DNA double stranded break repair defects[89]. Additional evidence for the loss-of-function hypothesis comes from studies showing that nuclear clearance of TDP-43 has the ability to exacerbate neurodegeneration in an Alzheimer's disease (AD) mouse model[90–92]. Research in Spinal Muscular Atrophy (SMA), a degenerative motor neuron disease, has similarly shown that loss of function of the RBP known as survival of motor neuron (SMN) results in abnormal processing of RNA, which contributes the pathogenesis of the disease. More recently, pathological studies using MS cortical tissue has revealed neuronal nuclear clearance of hnRNP A1, which is suggested to result in neurodegeneration in a manner similar to other RBPs in neurologic disease.

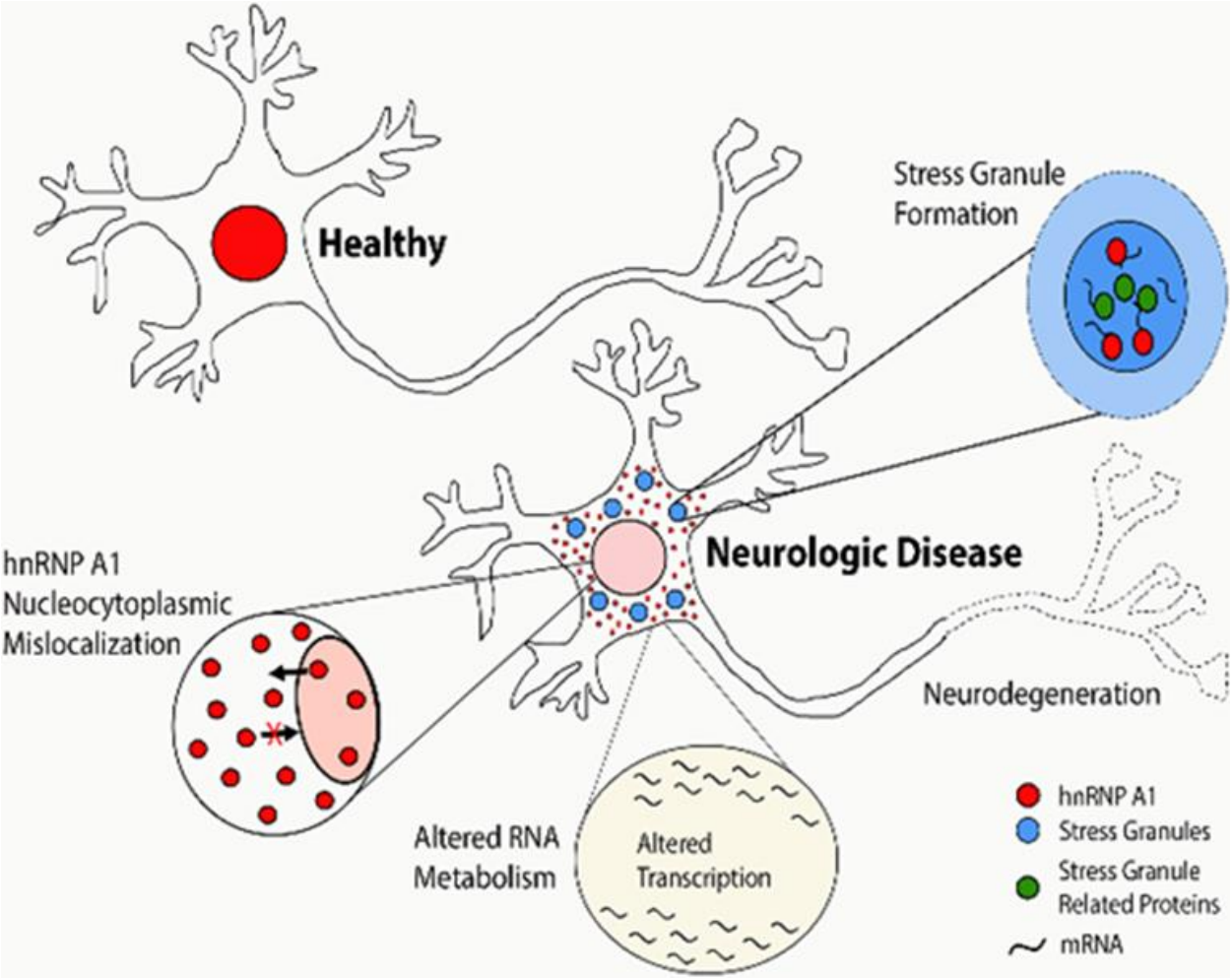

Figure 1.2 Schematic of the molecular consequences of RBP dysfunction. HnRNP A1 (red) is an RBP found to exhibit pathogenic features in ALS, FTLD and MS and is thought to underlie neurodegeneration. In healthy neurons, hnRNP A1 is predominantly nuclear. However, in neurologic disease, there is hnRNP A1 mislocalization from the nucleus to the cytoplasm, altered RNA metabolism and changes in SG formation, all of which cumulatively result in neurodegeneration. Adapted from [78].

1.4 Heterogeneous nuclear ribonucleoprotein A1

1.4.1 Structure and function

HnRNP A1 is a member of the largest family of RBPs known as heterogeneous nuclear ribonucleoproteins (hnRNPs), which are among one of the most diverse and widely expressed group of proteins in the nucleus[93–95]. There are currently two common validated splice variants of hnRNP A1, namely hnRNP A1-B (372 aa, 38kDa), known as the full-length isoform, and hnRNP A1-A (320aa, 34kDa), which is the shorter isoform. HnRNP A1-A is generally more abundant than the full-length isoform in most tissues[94].

The canonical structure of hnRNP A1 includes two RNA recognition motifs on the N-terminus, followed by a glycine rich domain on the C-terminus (Figure 1.3). Although the two RNA recognition motifs may seem structurally similar, they differ in amino acid sequences, which confers them different RNA-binding specificities[94,96]. Contained within the glycine-rich domain is a short sequence termed the RGG box RNA binding domain, which is a closely spaced sequence of Arg-Gly-Gly repeats and is thought to offer cooperative support to hnRNP A1 so that it can bind target RNA[97]. On the tail end of the glycine-rich domain is the nuclear localization sequence of hnRNP A1 termed the M9 sequence[94]. While hnRNP A1 is predominantly nuclear localized, it is also found to shuttle to and from the cytoplasm owing to its M9 sequence. Adding to hnRNP A1's functional diversity are post-translational modification sites, of which include phosphorylation, SUMOylation, ubiquitination, PARylation, acetylation and methylation cites[98]. These post translational modifications play an important role in controlling both functionality and localization of hnRNP A1.

The functional capabilities of hnRNP A1 are vast, as it is known to play a vital role in gene expression through controlling mRNA stability, regulation of translation as well as processing nascent transcripts through splicing[99,100]. Extending beyond its mRNA functions, hnRNP A1 also mediates nuclear export, processing of microRNA and telomere biogenesis[94,98,101,102]. Altogether, these functions make hnRNP A1 an important regulator in controlling normal cellular functioning and differentiation.

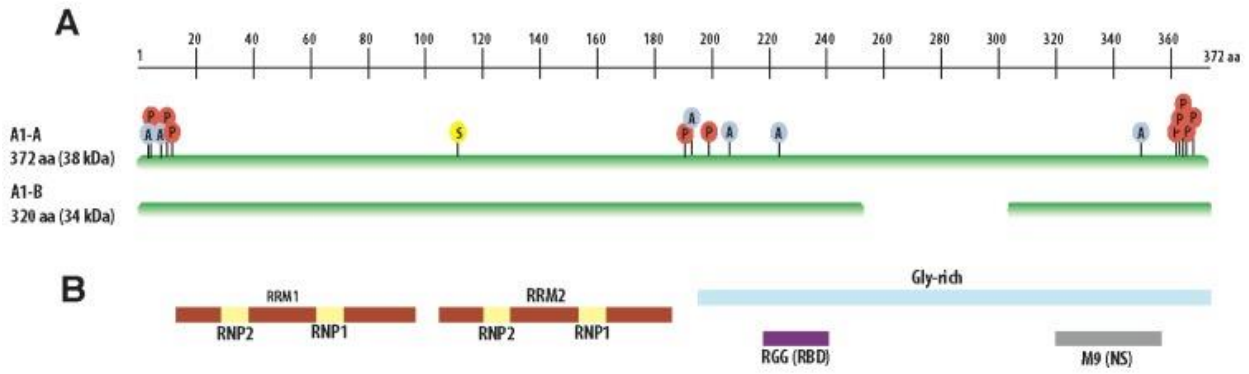

Figure 1.3 Structural features of hnRNP A1. *A,* Depiction of the 372 amino acid long isoform A1-A (38kDa) and the 320 amino acid long isoform A1-B (34kDa). Post-transcriptional sites are labelled as (A) acetylation, (P) phosphorylation and (S) SUMOylation. *B,* Representation of the functional domains of hnRNP A1: RRM1, RRM2 and the glycine-rich domain, which includes the RGG box and the M9 sequence. Adapted from [94].

1.4.2 Role in neurological diseases

HnRNP A1 is highly expressed in neurons and its dysfunction is a hallmark of several neurodegenerative diseases such as AD, ALS, FTLD and most recently MS[98,103–110]. Pathological features of hnRNP A1 dysfunction include its mislocalization from its homeostatic nuclear location to the cytoplasm, where hnRNP A1 has been found to form cytoplasmic inclusion bodies resulting in cellular dysfunction[76] and in severe cases, complete nuclear depletion[109,111,112]. Studies in ALS, FTLD and MS have revealed that these dysfunctional features are the culmination of disease-causing mutations and autoimmunity to hnRNP A1[54,60,91,103]. For example, mutations within the prion like domain of hnRNP A1 has been shown to result in increased mislocalization and consequently, cytoplasmic inclusions, dysregulated response to stress stimuli and stalled granule disassembly[95,98]. Levin et al.[54], additionally showed that patients with HTLV-1 associated myelopathy/tropical spastic paraparesis (HAM/TSP), a disease closely related to MS, make antibodies against hnRNP A1. Further experimentation utilizing hnRNP A1 antibodies and *ex vivo* brain slices, demonstrated the ability of hnRNP A1 antibodies to

decrease neuronal firing, ultimately alluding to their pathogenic involvement in disease[54,56].

The involvement of hnRNP A1 in the pathogenesis of neurodegeneration is further exemplified through studies in EAE, where hnRNP A1 antibodies resulted in worsened clinical disease and increased markers of neurodegeneration[56]. Additionally, examination of MS cortical neurons revealed a continuum of hnRNP A1 nucleocytoplasmic staining, where neurons from control patient samples exhibit physiologic nuclear hnRNP A1 localization and neurons from MS samples show pathologic hnRNP A1 nucleocytoplasmic mislocalization and nuclear depletion[109,110]. Widescale disruptions in RNA metabolism in AD and ALS have also been linked to reduced nuclear expression of hnRNP A1[111,112]. Altogether these studies demonstrate hnRNP A1 dysfunction and suggest that it is a novel contributor to the pathogenesis of neurodegeneration in diseases such as MS. However, thorough mechanistic links remain to be elucidated.

1.5 Stress granules

1.5.1 Structure and Function

SGs are a type of RNP granule that form in response to translation inhibition or cellular stress. Their composition consists of a stable core, which contains a concentrate of translationally stalled RNAs, translational machinery and RBPs, as well as an outer shell that is less concentrated and more fluid[113]. The formation of SGs is primarily driven by eukaryotic initiation factor 2 α (eIF2α) phosphorylation, or more recently discovered, an independent eIF2alpa phosphorylation pathway, which involves the disruption of eukaryotic initiation factor 4A (eIF4A)[114]. The end goal of these two pathways are to inhibit translation, whereby the act to release RNAs from translation machinery. The released RNAs then interact with RBPs and other misfolded proteins through liquid-liquid phase separation in the cytoplasm and drive the formation of the cytoplasmic inclusions, SGs[115].

Interestingly, nearly fifty percent of SG proteins are RBPs[113]. T-cell-restricted intracellular antigen-1 (TIA-1), Ras-GTPase-activating protein SH3-domain protein 1 (G3BP1) are two prime examples of RBPs that are core components required for SG formation[116]. It is believed that these proteins serve an integral role in SG assembly

whereby they interact with free RNA and act as a nuclear factor, driving the core formation of the SGs[116]. RBPs such as TDP-43 and hnRNP A1 have also been found to interact with SGs under stress conditions and exhibit the propensity to co-localize with SGs under pathologic conditions[110,117,118]. For example, a study by Guil et al.[117], demonstrated the physiological importance of hnRNP A1 in the stress response and its indispensable association with SGs. They showed that the knockdown of hnRNP A1 in HeLa cells significantly impacted the cells ability to recover from stress[117].

The overarching biological role of SGs is to sequester translationally stalled RNA and machinery during periods of stress, as to shift cellular energy away from translation thereby enabling the cell to recover from the stressor. After the dissipation of the stressor, cells resume homeostatic functioning as SGs begin to disassemble. In instances when the cells are unable to surmount the stressor, SGs aid in the induction of cellular death pathways[116].

1.5.2 Role in neurodegenerative diseases

The association between SGs and neurodegenerative disease largely originates from studies in ALS, FTLD and MS, where cytoplasmic aggregate formation is a prominent pathologic feature[109,119,120]. It is hypothesized that in these diseases, SG formation likely precedes protein aggregation, ultimately resulting in neurodegenerative consequences[119,120]. Further insight into pathology has revealed that mutational defects in RBPs such as TDP-43 and hnRNP A1, which commonly associate with SGs, can drive insoluble SG aggregate formation, and delay their disassembly[103]. Another common mutation in FTLD/ALS spectrum is that of C9ORF72, which has been shown to induce aggregate SGs and result in neurodegeneration[121]. Shedding light on the deleterious effects of these persistent SGs, Zhang P. et al.[122], utilized a novel light inducible system whereby G3BP, a core SG protein, was driven to form persistent SGs, which were shown to be toxic to the cells.

It is generally understood that although SGs serve a biologically important role in the stress response, changes in their core composition can accelerate their pathologic aggregation. One hypothesized explanation is that this leads to the continued sequestration of important RBPs, resulting in their diminished functioning within the cell,

which can further result in negative consequences for the health and survival of the cell[115,123,124].

1.6 Neuro-2a cells

1.6.1 Establishment and phenotype

The Neuro-2a cell line was first established by R.J Klebe and F.H Ruddle in 1969 from a spontaneous neuroblastoma in a strain A albino male mouse[125]. The morphology of this cell line is best described as amoeboid and neuronal-like, which has warranted its extensive use in research examining signaling pathways, axonal growth, and neuronal differentiation[126].

Of particular asset, Neuro-2a cells can rapidly differentiate into a more neuronal phenotype through the addition of factors such as cyclic AMP (cAMP), retinoic acid (RA), nerve growth factor (NGF), brain-derived neurotrophic factor (BDNF) or through serum deprivation[126]. The phenotypically differentiated Neuro-2a cells have increased neurofilaments and microtubular proteins[127]. The utilization of a specific differentiation method allows for these cells to display distinct neuronal qualities. For example, Tremblay et al.[126], showed that although factors such as transforming growth β 1 (TGFβ1), bone morphogenetic protein 4 (BMP4) and RA were sufficient to produce neuronal phenotypes, only the addition of dibutyryl cAMP significantly enhanced differentiation into dopamine neurons. This was evidenced through increased presence of both dopamine and tyrosine hydroxylase (TH), the rate limiting enzyme required in dopamine synthesis[126]. Although the exact mechanisms of neuronal differentiation are largely unknown, one study by Evanelopoulos et al.[128], was able to delineate the mechanism by which Neuro-2a differentiation occurred in serum withdrawal. It was found that serum deprivation led to the phosphorylation of the epidermal growth factor receptor (EGFR) pathway, resulting in increased neurites and morphological differentiation in Neuro-2a cells[128]. However, less is known about the subtype of neurons that are produced after serum withdrawal.

1.6.2 Model in disease

In addition to its use in elucidating mechanisms of cellular differentiation, Neuro-2a cells have also been utilized as models in neurologic diseases[129–131]. However, their

use has largely been limited to mechanistic studies due to limitations as a cell line as opposed to primary culture or *in vivo*. For example, the mechanism by which TDP-43 dysfunction induces neuronal damage was elucidated through the use of differentiated Neuro-2a cell lines[129]. Further, owing to their ability to differentiate into dopaminergic neurons, Neuro-2a cells have been readily utilized in Parkinson's disease (PD) and related mechanistic studies[126,129].

Interestingly, one study chose to query the use of Neuro-2a cells in motor neuron diseases such as ALS and SMA. Utilizing quantitative mass spectrometry-based proteomics, Hornburg et al.[132], compared the proteome of Neuro-2a cells to that of primary motoneurons and non-neuronal control cells. Their findings revealed that there were distinct differences in the proteins and pathways involved in differentiation[132]. Furthermore, they were able to show that there were also significant differences in the specific proteins known to be associated with ALS as compared to the primary motor neurons[132]. Although this study unveils the potential caveat to using cell lines such as Neuro-2a cells as a model for disease, no study has examined how these proteomic differences change once Neuro-2a cells have been differentiated.

1.7 Hypothesis and aims

Although hnRNP A1 dysfunction, particularly decreased hnRNP A1 nuclear expression, has been established as a prominent feature in MS and EAE neurons, the mechanistic link between how this loss-of-function phenotype results in neurodegeneration remains to be elucidated. Therefore, I hypothesize that decreased nuclear expression of hnRNP A1 will result in neurodegeneration in a model of MS (Figure 1.4). The hypothesis will be tested by the following aims:

1.7.1 Establish an *in vitro* model of decreased hnRNP A1 protein expression

An appropriate differentiation protocol for Neuro-2a cells will be established followed by evaluation of several hnRNP A1-specific siRNA oligonucleotides for their ability to decrease hnRNP A1 expression. Once validated, siRNA to hnRNP A1 will be transfected into differentiated Neuro-2a in order to establish a model of decreased hnRNP A1 expression.

1.7.2 Assess the effect of decreased hnRNP A1 protein expression on whole transcriptome expression

Utilizing the established model of decreased hnRNP A1 expression in Neuro-2a cells, RNA sequencing analysis will be performed, which will be followed by gene ontology (GO) enrichment analysis for pathways that are affected by decreased hnRNP A1 expression. To validate any downstream consequences of decreased hnRNP A1 expression, additional analysis evaluating the association of the differentially expressed (DE) transcripts and hnRNP A1 will be performed.

1.7.3 Assess downstream consequences of decreased hnRNP A1 protein expression on neuronal health, viability, and stress granule formation

Utilizing the established model of decreased hnRNP A1 expression in Neuro-2a cells, the detrimental effects of decreased hnRNP A1 expression will be evaluated by assessing neurite outgrowth, cell viability, related cellular death pathways and changes in the formation of SGs.

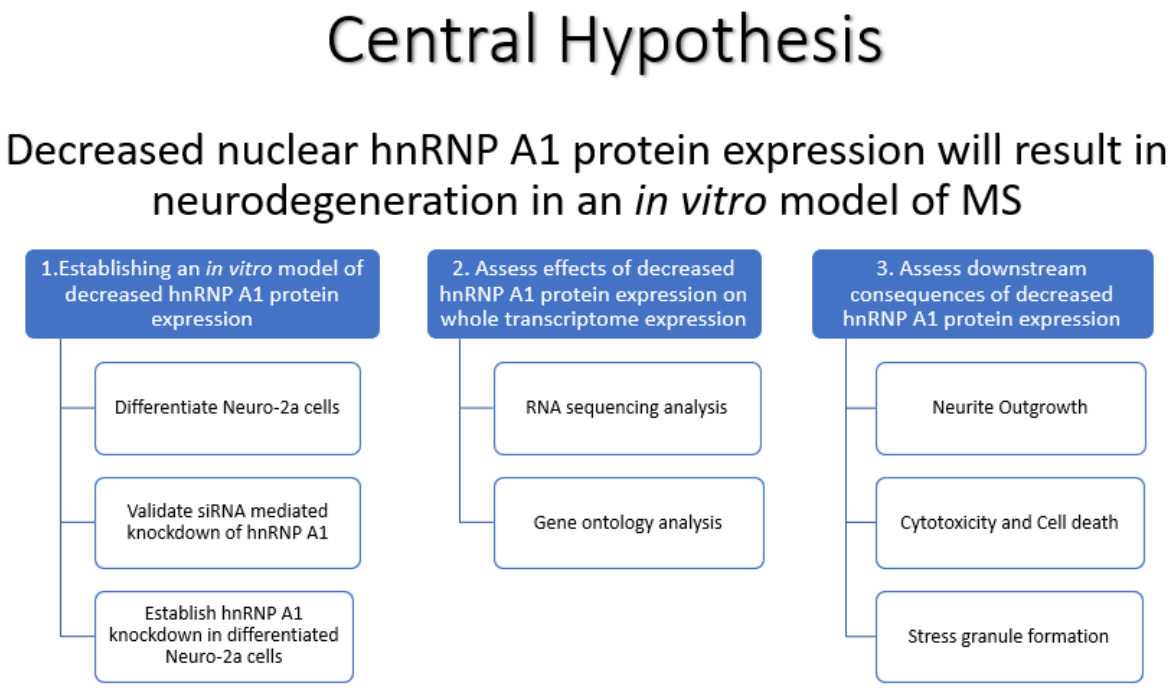

Figure 1.4 Summary of hypothesis and aims. The central hypothesis that 'Decreased nuclear hnRNP A1 protein expression will result in neurodegeneration in an *in vitro* model

of MS' will be tested through the following three aims: (1) Establishing an *in vitro* model of decreased hnRNP A1 protein expression by differentiating Neuro-2a cells, validating siRNA mediated knockdown of hnRNP A1, and establishing hnRNP A1 knockdown in differentiated Neuro-2a cells. (2) Assessing effects of decreased hnRNP A1 protein expression on whole transcriptome expression through RNA sequencing and gene ontology analysis. (3) Assessing downstream consequences of decreased hnRNP A1 protein expression on neurite outgrowth, cell death and stress granule formation.

CHAPTER 2: MATERIALS AND METHODOLOGY

2.1 Cell culture

2.1.1 Cell seeding and culture conditions

Neuro-2a cells (ATCC, CCL-131) are a mouse neuroblastoma cell line that were derived from a spontaneous tumor in a strain A albino mouse and display neuronal and amoeboid-like morphology[125]. Neuro-2a cells were maintained as a monolayer in complete media, which consisted of Dulbecco's modified eagle's medium (DMEM, Sigma cat. no. D6429), supplemented with 10% fetal bovine serum (FBS, Gibco cat. no. 12483-020), and 100U penicillin/streptomycin (Corning cat no. 30002CI) at 37ºC, in a humidified atmosphere containing 95% air and 5% CO_2. Cells were passaged at 80% confluency and were sub cultivated at a 1:5 ratio.

Prior to seeding Neuro-2a cells, all wells were coated with Poly-D-lysine hydrobromide (Sigma cat no. P6407) for 1 hour at 37ºC, after which wells were washed with double-distilled water (ddH_2O). For western blot experiments, cells were seeded into 6-well plates at a density of 300,000-500,000 cells per well. For immunocytochemistry experiments, cells were seeded into 8-well plates at a density of 25,000 cells per well. For assays requiring the use of 96-well plates, cells were seeded at a density of 10,000 cells per well. Trypan blue solution was used to count cells for seeding.

2.1.2 Differentiation conditions

Neuro-2a cells were plated in complete media and allowed to adhere for 24 hours before media was removed and changed to differentiation media. Cells were changed into the following differentiation media: DMEM, 100U penicillin/streptomycin and variable degrees of reduced serum (0.1%, 2% and 5% FBS) for 24 hours, DMEM, 100U penicillin/streptomycin, 10% FBS and variable concentrations of retinoic acid (RA, Sigma cat no. R2626) (1 µM, 5 µM, 10 µM and 20 µM RA) for 24 hours and DMEM, 100U penicillin/streptomycin, 2% FBS and 10 µM or 20 µM RA for 24, 48 and 72 hours. Cells were then fixed and analyzed (see **2.3.1 Immunocytochemistry protocol** and **2.6.1 Differentiation quantification**). Unless stated otherwise, DMEM, 100U

penicillin/streptomycin, 2% FBS and 10 µM RA was used to differentiate Neuro-2a cells and referred to as ‘differentiation media’.

2.1.3 siRNA transfections

The transfection of siRNA into Neuro-2a cells were performed using Lipofectamine RNAiMAX (Fisher Scientific cat no. 13778150) following manufacturer’s protocol for 16, 48 and 72 hours. For Neuro-2a cells plated in a 6-well, 8-well and 96-well plate, 25 pmol, 6.25 pmol and 1 pmol of final siRNA was used, respectively, for each well.

Table 2.1 siRNA oligonucleotide duplexes

siRNA Name	Target	Sequence	Manufacturer
siNEG	Non-targeting control	5’-UGGUUUACAUGUCGACAAA-3’	Integrated DNA Technologies
siA1#1	hnRNP A1	5’-GUGUAAAGUUAGUCUAUUC-3’	Integrated DNA Technologies
siA1#2	hnRNP A1	5’-GUGUGAAGUUAGAAUUCCU-3’	Integrated DNA Technologies
siA1#3	hnRNP A1	5’-GGUUAUAAAAUGGUUGUUG-3’	Integrated DNA Technologies
siA1#4	hnRNP A1	5’- GUAUCCAUUAUCAUGUGUA-3’	Integrated DNA Technologies
AlexaFluor647 siA1#4	hnRNP A1	5’-/5Alexa647N/GUAUCCAUUAUCAUGUGUA-3’	Integrated DNA Technologies

siCypB	Cyclophilin B (CypB)	5'-CCGUCGUCUUCCUUUUGCU-3', 5'-CUCUCGGAGCGCAAUAUGA-3', 5'-GAAAGAGCAUCUAUGGUGA-3', 5'-CCUAUACUUUGAUUUACAA-3'	Dharmacon

2.1.4 Sodium arsenite treatment

Sodium Arsenite is known to be a classical stressor, which has been well established in its ability to induce the formation of mammalian SGs[133]. Neuro-2a cells were plated in an 8-well plate and were allowed to adhere for 24 hours before treatment. Cells were transfected with siRNA (see **2.1.3 siRNA transfections**) for 16 hours before media was changed into differentiation media. After 72 hours of siRNA transfection, Neuro-2a cells were treated with 0.5 mM sodium arsenite (Sigma cat no. 1062771003) for 30 minutes at 37ºC and were then fixed and analyzed (see **2.3.1 Immunocytochemistry protocol** and **2.6.5 Stress granule quantification**).

2.2 Protein Analyses

2.2.1 Cell culture harvest

Neuro-2a cells were harvested for protein analyses by scraping wells using a cell scraper (Fisher Scientific cat no. 08-100-241). Cell suspension was collected in a 50 mL conical tube and an additional 10-15 mL complete media was added to cell suspension before being centrifuged at 300 x g for 5 minutes. The supernatant was discarded, and the pellet was resuspended in 10-15 mL phosphate buffered saline (PBS) and centrifuged at 300 x g for 5 minutes. The supernatant was discarded again, and the pellet was resuspended in 10-15 mL PBS for a second wash and centrifuged at 300 x g for 5 minutes. The supernatant was discarded, and the pellet was resuspended in a volume of cytobuster protein extraction reagent (Fisher Scientific cat no. 71-009) and Halt protease inhibitor cocktail (100X, Fisher Scientific cat no. PI87786). For 5 mL of cytobuster protein extraction reagent, 50 µL of 100X Halt protease inhibitor cocktail was used. After pellet resuspension, suspensions were agitated for 5 minutes, before being centrifuged at

16,000 x g at 4ºC for 5 minutes. The supernatants (cell lysate) were kept at -80ºC for further analyses.

2.2.2 Nuclear Cytoplasmic Fractionation

Neuro-2a cells were harvested by scraping using a cell scraper and resuspended in 10-15 mL complete media being before centrifuged at 300 x g for 5 minutes. The cell pellet was resuspended in 1 mL PBS and transferred to a 1.5 mL microcentrifuge tube before being centrifuged at 300 x g for 3 minutes. The supernatant was discarded, and the pellet was allowed to dry. The NE-PER Nuclear and Cytoplasmic Extraction Reagents (Thermo Scientific cat no. 78833) were used to extract nuclear and cytoplasmic fractions following manufacturer's protocol. The supernatants were kept at -80ºC for further analyses.

2.2.3 Acetone precipitation

The required amount protein for each experiment was determined using a NanoDrop spectrophotometer (Thermo Scientific cat no. ND-2000). The predetermined amount of lysate was added to five times the volume of ice-cold acetone and was briefly vortexed before being incubated at -20ºC for 20 minutes. Following incubation, samples were centrifuged at 18,000 x g at 4ºC for 20 minutes. Supernatants were discarded and pellets were allowed to air dry and an appropriate volume of 1X sample buffer was added to each sample. Samples were briefly vortexed and placed in a heat block at 95ºC for 5 minutes and were then loaded onto polyacrylamide gels.

2.2.4 Polyacrylamide gels

Polyacrylamide gels were made at percentages and volumes listed in Table 2.2.

Table 2.2 Acrylamide Gel volumes and reagents

Resolving Gel	
10%	**Reagent**
3.8 mL	ddH_2O
2 mL	40% Acrylamide
2 mL	1.5 M Tris, pH 8.8

80 µL	10% Sodium dodecyl sulfate
80 µL	10% Ammonium persulfate
8 µL	Tetramethylethylenediamine

Stacking Gel	
6%	**Reagent**
3.525 mL	ddH_2O
750 µL	40% Acrylamide
625 µL	1.0 M Tris, pH 6.8
50 µL	10% Sodium dodecyl sulfate
50 µL	10% Ammonium persulfate
5 µL	Tetramethylethylenediamine

The resolving gel was allowed to polymerize for 1 hour before the stacking gel was added along with a well comb. Once the gels were fully polymerized, the polyacrylamide gels were set into the electrophoresis cassette and 1X running buffer was poured to fill. The combs were then removed and the samples in 1X sample buffer were loaded into the appropriate wells. The Precision Plus Protein ™ WesternC ™ Blotting Standard (Bio-Rad cat no. 1610385) was used as a ladder and 1X sample buffer was loaded into any unused wells. The gels were then run at 120V for 2 hours.

2.2.5 Western blotting protocol

To prepare for semi-dry transfer, immobilin-P PVDF membrane (Sigma cat no. IPVH00010) was soaked in ice-cold methanol for 5 minutes before being rinsed in ddH_2O. The PVDF membrane along with Western Blotting Filter Papers (Fisher Scientific cat no. PI88605) was then soaked in cold transfer buffer for 15 minutes. Once the gel was finished running, it was gently removed and allowed to soak in cold transfer buffer for 30 minutes. Following soaking, the filter paper, PVDF membrane and gel was assembled for transfer and bubbles were removed by gently rolling using a 15 mL conical tube. The gel was transferred at 10V for 30 minutes.

Following transfer, membranes were placed in 10% normal goat serum (Jackson ImmunoResearch cat no. 005-000-121) for 1 hour at room temperature or overnight at 4ºC. Membranes were then briefly washed in 10mM TBS + 0.1% Tween-20 (TBST) and then incubated in primary antibody diluted in TBST for 1 hour at room temperature or overnight at 4ºC, on a shaker. Primary antibody incubation was followed by another brief wash in TBST and incubation in secondary antibodies diluted in TBST for 1 hour at room temperature on a shaker. Membranes were then briefly washed in TBST and 10mM TBS, followed by development of membranes in clarity western enhanced chemiluminescence (ECL) substrates (Bio-Rad cat no. 1705060S) for 5 minutes. Membranes were then scanned on the ChemiDoc™ imaging system (BioRad).

2.2.6 Primary antibodies for western blotting

Table 2.3 Primary antibodies used for western blot

Target	Species	Catalog No.	Dilution
β-Actin	Mouse	Cell Signaling Technology #3700S	1:1000
β-Actin	Rabbit	Cell Signaling Technology #4967S	1:1000
hnRNP A1 (9H10)	Mouse	Millipore Sigma #04-1469	1:1000
hnRNP A1 (4B10)	Mouse	Millipore Sigma #05-1521	1:1000
CypB	Rabbit	Abcam #ab16045	1:500
Lamin B1 (B-10)	Mouse	Santa Cruz #sc374015	1:100

2.2.7 Secondary antibodies for western blotting

Table 2.4 Secondary antibodies used for western blot

Target	Species	Catalog no.	Dilution
Anti- Mouse IgG (H+L) HRP Conjugate	Goat	Bio-Rad #1706516	1:3000
Anti-Rabbit IgG (H+L) HRP Conjugate	Goat	Bio-Rad #1706515	1:3000
Precision Protein StrepTactin-Horseradish Peroxidase Conjugate	Cattle	Bio-Rad #1610381	1:10,000

2.3 Immunocytochemistry

2.3.1 Immunocytochemistry protocol

Neuro-2a cells were fixed with 3.7% formaldehyde diluted in complete media at 37ºC for 15 minutes. Following fixation, cells were briefly washed in PBS and permeabilized in ice cold acetone at -20ºC for 5 minutes. Cell were then briefly washed in PBS and blocked in 100% Seablock for 1 hour at room temperature. Subsequently, cells were briefly washed with PBS + Triton-X 100 (PBS-T, 0.1%) and incubated in primary antibody for 1 hour at room temperature or 4ºC overnight. Primary antibodies were diluted in 10% Seablock PBS-T (0.1%). Following primary antibody incubation, cells were briefly washed again with PBS-T (0.1%) and incubated in secondary antibody for 30 minutes at room temperature. Secondary antibodies were diluted in 5% Seablock PBS. Lastly, cells were briefly washed with PBS and 8-well chambers were removed and slides were mounted with either Prolong Gold antifade reagent (Fisher Scientific cat no. P36934) or ProLong Gold antifade reagent with DAPI (Fisher Scientific cat no. P36935).

2.3.2 Primary antibodies for immunocytochemistry

Table 2.5 Primary antibodies used for immunocytochemistry

Target	Species	Catalog no.	Dilution
Neurofilament (NF-L, pan-neuronal, SMI 311)	Mouse	Biolegend #837801/2	1:1000
hnRNP A1 (9H10)	Mouse	Abcam #ab5832	1:500
hnRNP A1	Rabbit	Abcam #ab4791	1:500
β-III-Tubulin	Rabbit	Sigma #T2200	1:1000
β-III-Tubulin	Chicken	Aves Labs #TUJ	1:500
Ras-GTPase-Activating Protein SH3 domain binding protein (G3BP)	Rabbit	Abcam #ab181149	1:500
pMLKL	Rabbit	Novus Biologicals #NBP2-66953	1:500

2.3.3 Secondary antibodies for immunocytochemistry

Table 2.6 Secondary antibodies used for immunocytochemistry

Target	Species	Catalog no.	Dilution
Mouse Alexa Fluor 488	Donkey	Jackson ImmunoResearch #016-540-084	1:1000
Rabbit Alexa Fluor 594	Goat	Jackson ImmunoResearch #111-586-042	1:1000
Chicken DyLight 405	Donkey	Jackson ImmunoResearch #703-475-155	1:500

2.4 RNA sequencing analyses

2.4.1 RNA extraction

Neuro-2a cells were harvested under RNase free conditions by scraping wells using a cell scraper. Cell suspension was collected in a 50 mL conical tube and an additional 10-15 mL complete media was added to cell suspension before being centrifuged at 300 x g for 5 minutes. The supernatant was discarded, and the pellet was resuspended in 10-15 mL PBS and centrifuged at 300 x g for 5 minutes. The supernatant was discarded again, and the pellet was resuspended in 10-15 mL PBS for a second wash and centrifuged at 300 x g for 5 minutes. Following centrifugation, the RNeasy Plus Mini Kit (Qiagen cat no. 74136) was used to extract RNA following manufacturer's protocol. RNA was eluted using RNase free water and quality of RNA was verified using the Nanodrop spectrophotometer. RNA samples were kept in -80ºC for further analyses.

2.4.2 Library Preparation

RNA sequencing libraries were generated using 10 ng of input RNA using the Ovation SoLo RNA-Seq Systems (Tecan Genomics cat no. 0407-32) following manufacturer's directions.

2.4.3 RNA sequencing

Sequencing libraries were quantified using a Qubit 4.0 fluorometer (Invitrogen, Thermo Fisher Scientific Waltham, MA, USA) and Qubit 1X dsDNA HS assay (Invitrogen). The library fragments length distributions were determined using a TapeStation 4150 instrument (Agilent, Santa Clara, CA, USA) with D1000 ScreenTape and reagents (Agilent). The barcoded libraries were pooled equimolar and 75 bp paired end reads generated on a NextSeq 550 instrument (Illumina, San Diego, CA, USA).

For differential gene expression, the reads were extracted from each run and adapter trimmed using bcl2fastq (version 2.19.0.316; Illumina) with the following settings: "--use-bases-mask Y*,I8Y*,Y* --minimum-trimmed-read-length 0 --mask-short-adapter-reads 0". Sequencing adapters and low-quality bases were trimmed using fastp[134] with default settings except the following: "-f 5 -Y 0 -g". The reads were aligned to the GRCm38

mouse reference genome[135] using STAR (version 2.5.1b)[136] with default settings and keeping only unique alignments. Duplicate reads were identified and discarded using the NuDup tool (version 2.3; Tecan Genomics) using information from the unique molecular identifiers (UMIs) extracted from the index reads and read alignments. Gene-level expression was determined using htseq-count from the HTSeq framework (version 0.11.3)[137] with default settings except for: "--nonunique all". Genes that were differentially expressed (DE) between the control and siRNA-treated samples were identified using DESeq2 (version 1.22.2)[138] in R (version 3.6.1)[139]. Significance was considered at a Benjamini-Hochberg adjusted p-value threshold of 0.05.

2.4.4 Gene ontology analyses

DE genes were analyzed using Cytoscape software (v. 3.8.2)[140], including the STRING protein query to obtain protein-protein interaction networks. Gene Ontology (GO) enrichment analysis was performed using STRING enrichment analysis software[141].

2.4.5 Differentially expressed gene transcript binding analyses

Known RNA binding partners of hnRNP A1 in human were identified using CLIPdb[142], a database with over 300 publicly available UV-crosslinking immunoprecipitation and sequencing (CLIPseq) datasets identifying interactions between RBPs and target RNA. DE genes were converted to human orthologs using the ensembl tool[143] and compared to the data acquired from CLIPdb.

2.5 Assays

2.5.1 Lactate dehydrogenase assay

Neuro-2a cells were plated in a 96-well plate and were allowed to sit for 24 hours before treatment. Cells were transfected with siRNA (see **2.1.3 siRNA transfections**) and were allowed to sit for 16 hours before media was changed into differentiation media. After 72 hours of siRNA transfection, cell cytotoxicity was measured using the CyQUANT ™ lactate dehydrogenase (LDH) cytotoxicity assay (Fisher Scientific cat no. C20300) according to manufacturer's directions. Three experimental replicates were performed with each condition performed in triplicate. Absorbance was measured at 680 nm and

490 nm using a spectrophotometer microplate reader. LDH activity was calculated through the subtraction of the absorbance at 680 nm from the absorbance at 490 nm. Percent cytotoxicity was calculated using the following formula:

$$\%\text{Cytotoxicity}=\left[\frac{Experimental\ group\ LDH\ activity-Spontaneous\ LDH\ activity}{Maximum\ LDH\ activity-Spontanous\ LDH\ activity}\right] \times 100$$

2.5.2 Caspase 3/7 assay

Neuro-2a cells were plated in a 96-well plate and were allowed to sit for 24 hours before treatment. Cells were transfected with siRNA (see **2.1.3 siRNA transfections**) and were allowed to sit for 16 hours before media was changed into differentiation media. After 72 hours of siRNA transfection, caspase 3/7 activity was measured using the Apo-ONE homogeneous caspase 3/7 assay (Promega cat no. G7790) following manufacturer's directions. Three experimental replicates were performed with each condition performed in triplicate. Fluorescence of each well was measured at an excitation wavelength of 499 nm and an emission wavelength of 521 nm using a spectrophotometer microplate reader.

2.6 Data analysis

2.6.1 Differentiation quantification

Images of differentiated Neuro-2a cells were acquired at 40x objective, with a 1.40 numerical aperture, on a Axio Observer 7, inverted fluorescent microscope (Carl Zeiss Canada Ltd., Toronto, ON, Canada). Images were prepared for quantification using ZEN 3.2 Blue Edition software (Carl Zeiss Canada Ltd., Toronto, ON, Canada). The DAPI images were opened in Adobe photoshop and were used to randomly select 10 cells per condition using the counter tool. The corresponding NF-L images were opened in ImageJ software and were converted to 8-bit grey-scale images. The scale was set on ImageJ using a scale bar and the 8-bit grey-scale images were then imported to the NeuronJ[144] plugin for ImageJ. NeuronJ was used to trace the neurites of the randomly selected cells in each condition, giving readings of neurite sum length (μm) for each cell. Statistical analyses were performed using GraphPad Prism 9 software. For multiple comparisons,

one-way ANOVA with Bonferroni post-hoc tests were used to determine statistical significance. $P<0.05$ was considered statistically significant.

2.6.2 Western blot

ImageJ software was used to calculate signal intensity for each western blot. For each protein that was tested, the relative signal intensity was calculated relative to the control group signal and was normalized to the loading control (β-actin or lamin B1). The relative change in signal intensity of the treatment groups was compared to that of the control group for each protein. Statistical analyses were performed using GraphPad Prism 9 software. For comparisons between treatment and control groups, one-tailed unpaired t-tests were used to determine statistical differences. $P<0.05$ was considered statistically significant.

2.6.3 Fluorescence quantification

Images of differentiated Neuro-2a cells treated with siRNA and/or subsequent treatment with sodium arsenite were acquired at 20x or 40x objective, with a 1.40 numerical aperture, on a Axio Observer 7, inverted fluorescent microscope. Images were prepared for quantification using ZEN 3.2 Blue Edition software. Images were individually opened on ImageJ software and were merged using the merge channel tool. For conditions with DAPI staining, the DAPI images were used to trace nuclei of cells to generate regions of interest (ROIs) to quantify corrected total hnRNP nuclear fluorescence. For conditions with no DAPI staining, the β-III-tubulin images were used to trace the entire cell to generate ROIs to quantify corrected total hnRNP A1 cellular fluorescence. ROIs from the DAPI or β-III-tubulin images were overlaid onto hnRNP A1 images, and the raw integrated density was recorded for each ROI. Background readings were recorded next to each ROI for normalization. Corrected total hnRNP A1 nuclear or cellular fluorescence was calculated using the following formula:

$$\text{Corrected total A1 nuclear or cellular fluorescence} = Raw\ Integrated\ Density - (Area\ of\ selected\ cell \times Mean\ fluorescence\ of\ background\ readings)$$

2.6.4 Neurite outgrowth quantification

Images of differentiated Neuro-2a cells treated with siRNA were acquired at 20x objective, with a 1.40 numerical aperture, on a Axio Observer 7, inverted fluorescent microscope. Images were prepared for quantification using ZEN 3.2 Blue Edition software. The DAPI images were opened on Adobe photoshop and were used to randomly select 30 cells per condition using the counter tool. The β-III-tubulin images were opened in ImageJ and were converted to 8-bit grey-scale images. The scale was set on ImageJ using a scale bar and the 8-bit grey-scale images were then imported to NeuronJ[144], which was used to trace neurites of the randomly selected cells. Three experimental replicates were performed for each condition. Readings of neurite branch number and neurite sum length (μm) were recorded for each cell. Corrected total hnRNP A1 nuclear fluorescence was measured according to **2.6.3 Fluorescence quantification**. Cells in the siA1 treated group were assessed for greater than 50% knockdown of hnRNP A1 and were used to quantify differences in neurite sum length and branching against the control group. Average corrected total hnRNP A1 nuclear fluorescence of the control group was used for normalization. Statistical analyses were performed using GraphPad Prism 9 software. For comparisons between treatment and control groups, one-tailed unpaired t-tests were used to determine statistical differences. $P<0.05$ was considered statistically significant. Pearson's correlation test was used for correlation analyses.

2.6.5 Stress granule quantification

Images of differentiated Neuro-2a cells treated with siRNA followed by sodium arsenite treatment were acquired at 40x objective, with a 1.40 numerical aperture, on a Axio Observer 7, inverted fluorescent microscope. Images were prepared for quantification using ZEN 3.2 Blue Edition software. The β-III-tubulin images were opened on Adobe photoshop and were used to randomly select 90 cells per condition using the counter tool. The G3BP images were opened on ImageJ and converted to 8-bit grey-scale images. The scale was set on ImageJ using a scale bar. Each randomly selected cell was outlined and duplicated onto another window for puncta analysis. Individual cells were processed through bandpass filter to 20 pixels, followed by thresholding to visualize individual puncta. The analyze particle tool was used to give readouts of the size of puncta and the number of puncta within each individual cell. Three experimental replicates were

performed for each condition. Corrected total hnRNP A1 cellular fluorescence was measured according to **2.6.3 Fluorescence quantification**. Cells in the siA1 treated group were assessed for greater than 50% knockdown of hnRNP A1 and were used to quantify differences in SG size and number against the control group. Average corrected total hnRNP A1 cellular fluorescence of the control group was used for normalization. Statistical analyses were performed using GraphPad Prism 9 software. For comparisons between treatment and control groups, one-tailed unpaired t-tests were used to determine statistical differences. $P<0.05$ was considered statistically significant. Pearson's correlation test was used for correlation analyses.

2.6.6 Necroptosis quantification

Images of differentiated Neuro-2a cells treated with siRNA were acquired at 40x objective, with a 1.40 numerical aperture, on a Axio Observer 7, inverted fluorescent microscope. Images were prepared for quantification using ZEN 3.2 Blue Edition software. The β-III-tubulin channel was opened onto Adobe photoshop and was used to randomly select 100 cells in each replicate per condition. The pMLKL channel was then used to qualitatively categorize the randomly selected cells into groups of cells that possessed diffuse pMLKL staining or non-diffuse punctate staining. Three experimental replicates were performed for each condition. Statistical analyses were performed using GraphPad Prism 9 software. For comparisons between treatment and control groups, one-tailed unpaired t-tests were used to determine statistical differences. $P<0.05$ was considered statistically significant.

CHAPTER 3: RESULTS

3.1 Knockdown of hnRNP A1 in differentiated Neuro-2a cells as a loss-of-function model

Decreased hnRNP A1 expression is a pathologic feature observed in MS tissue and EAE disease, and is thought to underlie neurodegeneration[10,56,78,95,108–110]. To model this dysfunction in vitro, we employed siRNA genetic knockdown in differentiated Neuro-2a cells.

3.1.1 siA1#4 results in most potent knockdown of hnRNP A1

To optimize hnRNP A1 knockdown, four different siRNA oligonucleotides targeting different regions of hnRNP A1 mRNA were tested (siA1#1-4; Figure 3.1A) for their efficiency to knockdown hnRNP A1. Transfections were performed for 72 hours in undifferentiated Neuro-2a cells before harvesting cell lysates for western blotting (Figure 3.1B). Figure 3.1C, D illustrates that siA1#4 was the most potent siRNA targeting hnRNP A1 as compared to the control non-targeting siRNA (siNEG). Therefore, siA1#4 was chosen for all subsequent experiments (herein referred to as siA1).

3.1.2 Combination of reduced serum and retinoic acid differentiates Neuro-2a cells

Neuro-2a cells have been extensively used to study neuronal differentiation, axonal growth and signaling pathway[126]. They have the convenient characteristic of being easy to differentiate into cells with neuronal morphology in different culture conditions. Reduced serum and the addition of RA are the most widely used conditions for Neuro-2a differentiation[126,129,145], however there is a lack of consensus as to which condition is the most ideal. Therefore, it was pertinent to test various conditions to decide which differentiation conditions were the most ideal for downstream application.

Neuro-2a cells were cultured in 0.1%, 2%, 5 % and 10% FBS for 24 hours, followed by fixation and immunostaining for hnRNP A1 and NF-L, which stained neuronal processes (Figure 3.2A). Quantification revealed that cells in the 10% FBS condition (ie. no serum withdrawal) exhibited little to no differentiation, evident through the lack of neurites. Cells in the serum deprived conditions began developing small neurites, with

cells in the 2% FBS condition having the longest neurites, while cells in the 0.1% and 5% FBS condition had smaller neurites (Figure 3.2B, C). However, it is important to note that a large proportion of cells within all the serum deprived conditions remained undifferentiated. This led us to query the use of RA to differentiate Neuro-2a cells.

Neuro-2a cells were then cultured in 1µM, 5µM, 10µM and 20µM RA diluted in complete media for 24 hours. Cells were then fixed and immunostained for hnRNP A1 and NF-L. Quantification revealed that cells in the 10µM and 20µM RA conditions exhibited the longest neurites as compared to the cells in the 1µM and 5µM RA differentiation conditions (Figure 3.3A, B). Like the FBS differentiation conditions, a large proportion of the cells remained undifferentiated, hence an alternative differentiation condition was explored.

Some studies reported the combinatorial use of serum withdrawal and RA to fully differentiate Neuro-2a cells[129,145]. Particularly, the study by You et al. 2020[145] tested the use of 2% FBS and 10µM or 20µM RA for 24-120 hours as differentiation conditions for Neuro-2a cells. They noted that the duration of differentiation, in addition to the specific differentiation media, was an important factor. For example, they observed that increasing the duration Neuro-2a cells were cultured in the differentiation media, resulted in significantly greater number and length of neurites. Further, they reported that 2% FBS in combination with 20µM RA was toxic to the cells, therefore, they decided to use the 2% FBS in combination with 10µM RA for all their subsequent experiments.

To confirm this reported observation by You et al. (2020)[145], Neuro-2a cells were cultured in 2% FBS in combination with 10µM or 20µM RA for 24, 48 and 72 hours to determine the ideal differentiation condition (Figure 3.4A). Similarly, immunofluorescent imaging and neurite length quantification revealed that increased duration of differentiation resulted in increased neurite length (Figure 3.4B, C). This observation was consistent for both RA concentrations. However, there were fewer cells in the conditions with 20µM RA, which suggested that this higher concentration of RA was toxic to the cells and resulted in cell death. Thus, for all subsequent experiments, cells were differentiated in 2% FBS in combination with 10µM RA for 72 hours, as this condition produced the longest neurites.

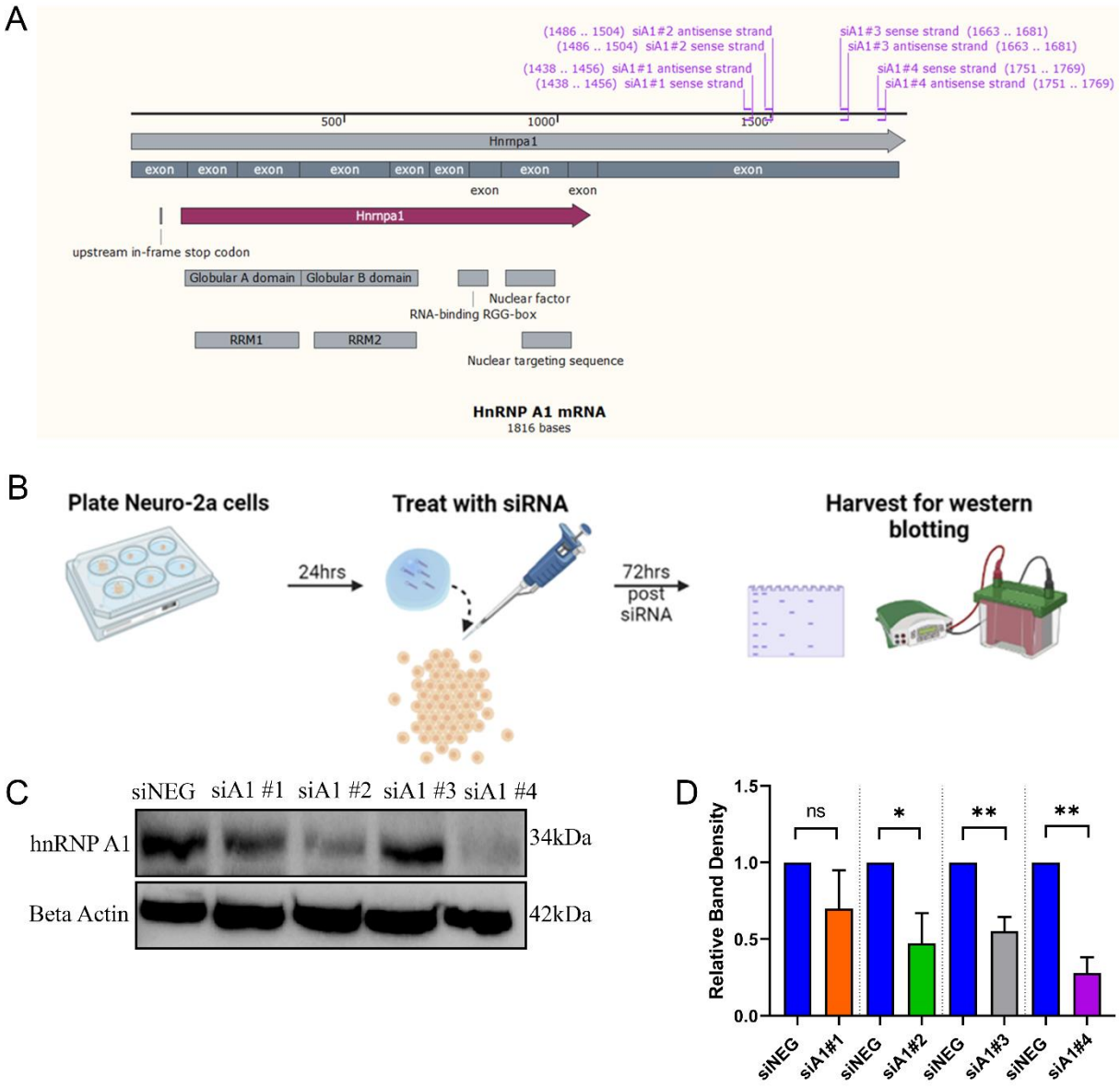

Figure 3.1 siA1#4 results in the most potent knockdown of hnRNP A1 in undifferentiated Neuro-2a cells. *A*, siA1#1-4 target different regions of hnRNP A1 mRNA. *B*, Neuro-2a siRNA transfection and data collection protocol. *C*, Undifferentiated Neuro-2a cells were treated with 4 different siA1 duplex oligonucleotides for 72 hours, which showed varying degrees of hnRNP A1 knockdown. *D*, Quantification of (C) demonstrating siA1#4 was the most potent siA1 duplex oligonucleotide to significantly decrease hnRNP A1 expression compared to siNEG. Unpaired t-test (ns= non-significant, *p<0.05, **p<0.01); n=3 biological replicates; Data are plotted as mean ± SEM.

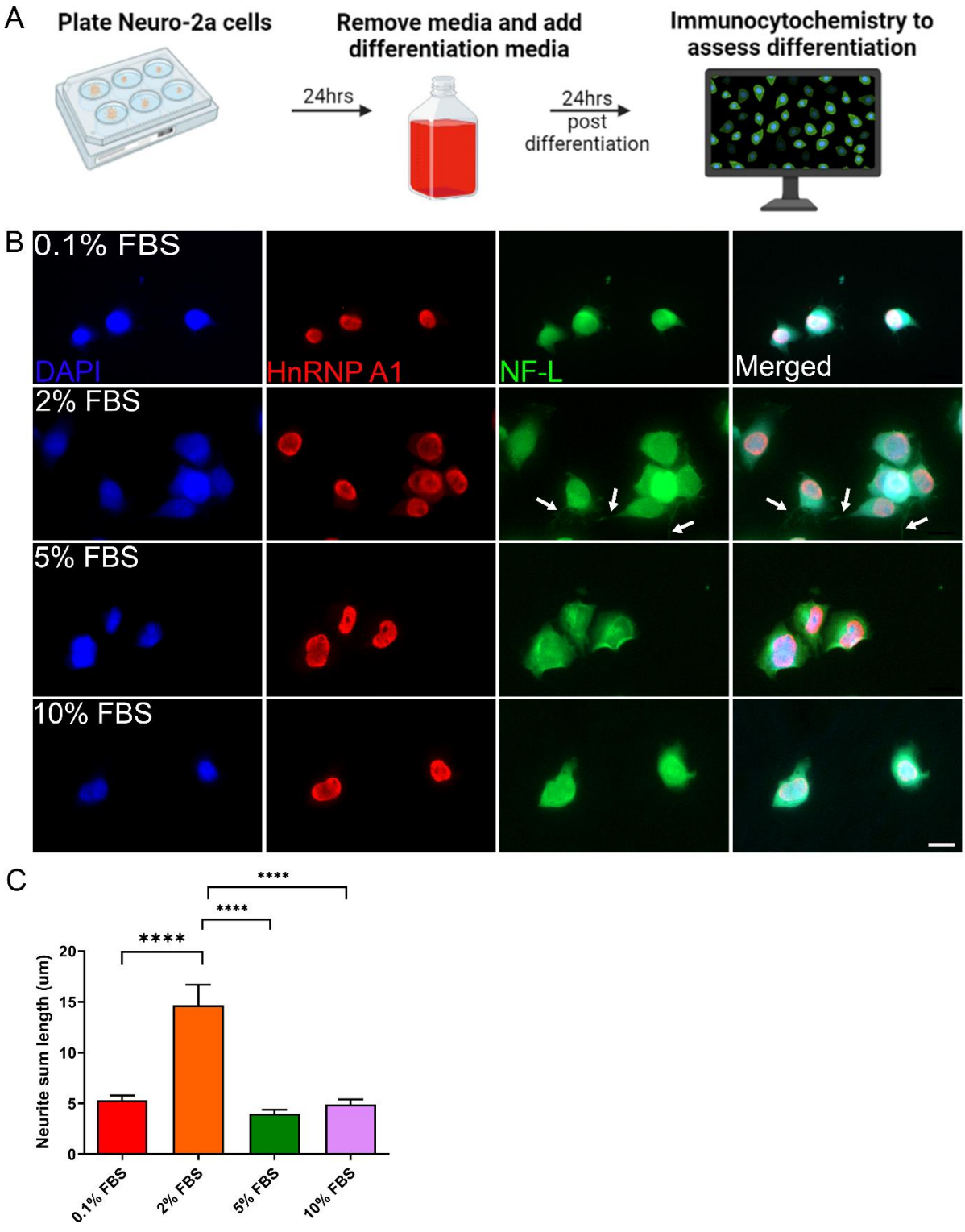

Figure 3.2 Differentiation of Neuro-2a cells in serum deprived media. *A*, Neuro-2a differentiation and data collection protocol. *B,* Neuro-2a cells cultured in 0.1%, 2%, 5% or

10% FBS for 24 hours stained for DAPI (blue), hnRNP A1 (red) and NF-L (green). Scale bar = 20μm. Classification of differentiation was evaluated quantitatively through NF-L, which identifies neuronal processes. Arrows (white) indicate representative processes of differentiated Neuro-2a cells found in the 2% FBS condition. *C,* Quantification revealed that Neuro-2a cells cultured in 2% FBS resulted in the longest processes compared to 0.1%, 5% and 10% FBS differentiation conditions. One-way ANOVA (****$p<0.0001$); n=10 cells per condition. Data are plotted as mean ± SEM.

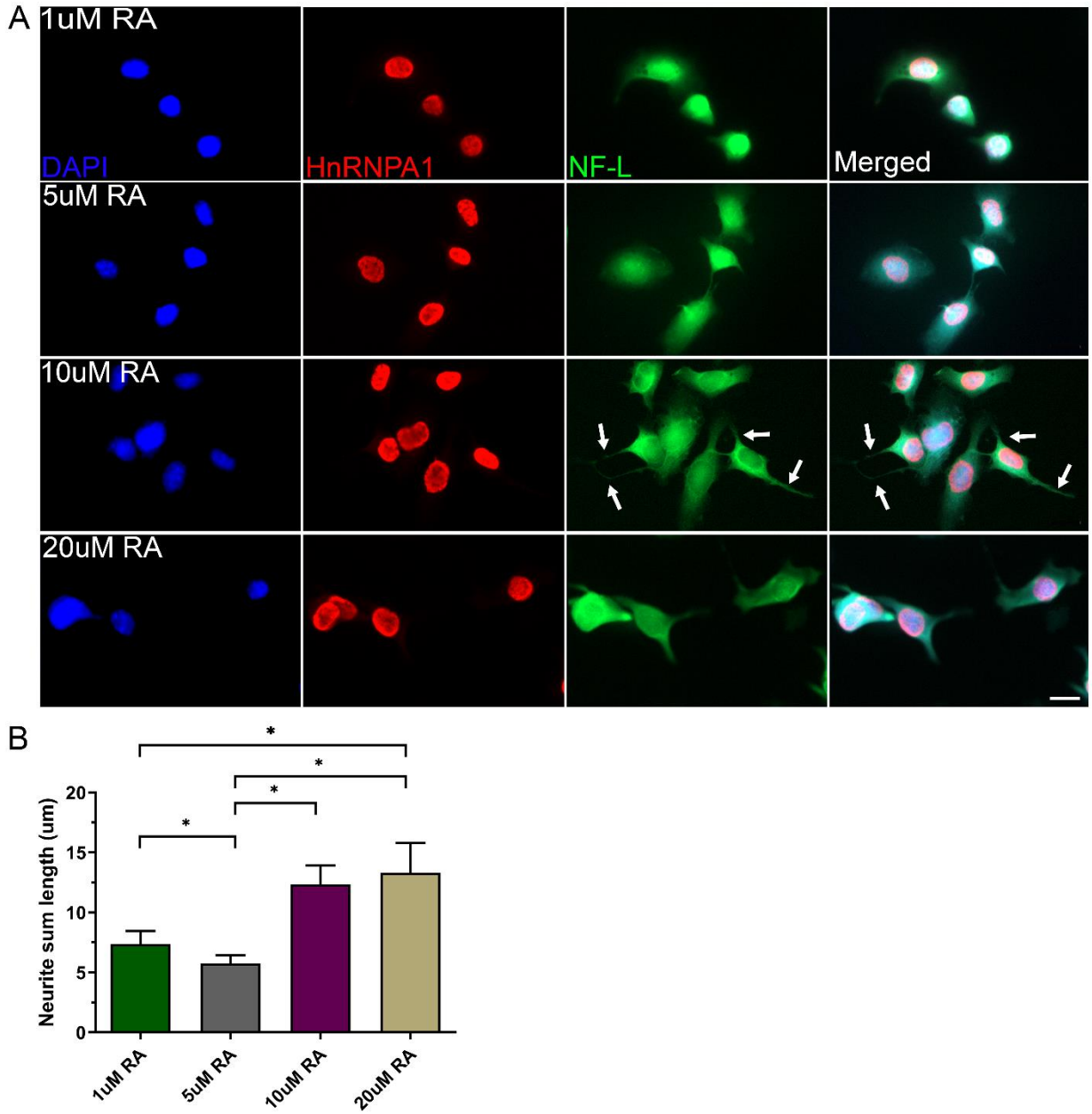

Figure 3.3 Differentiation of Neuro-2a cells in RA. *A,* Neuro-2a cells cultured in 1µM, 5µM, 10µM and 20µM RA for 24 hours stained for DAPI (blue), hnRNP A1 (red) and NF-L (green). Scale bar = 20µm. Classification of differentiation was evaluated quantitatively through NF-L, which identifies neuronal processes. Arrows (white) indicate representative processes of differentiated Neuro-2a cells found in the 10µM RA condition. *B,* Quantification revealed that Neuro-2a cells cultured in 10µM and 20µM RA conditions exhibited the longest processes. One-way ANOVA (*p<0.05); n=10 cells per condition. Data are plotted as mean ± SEM.

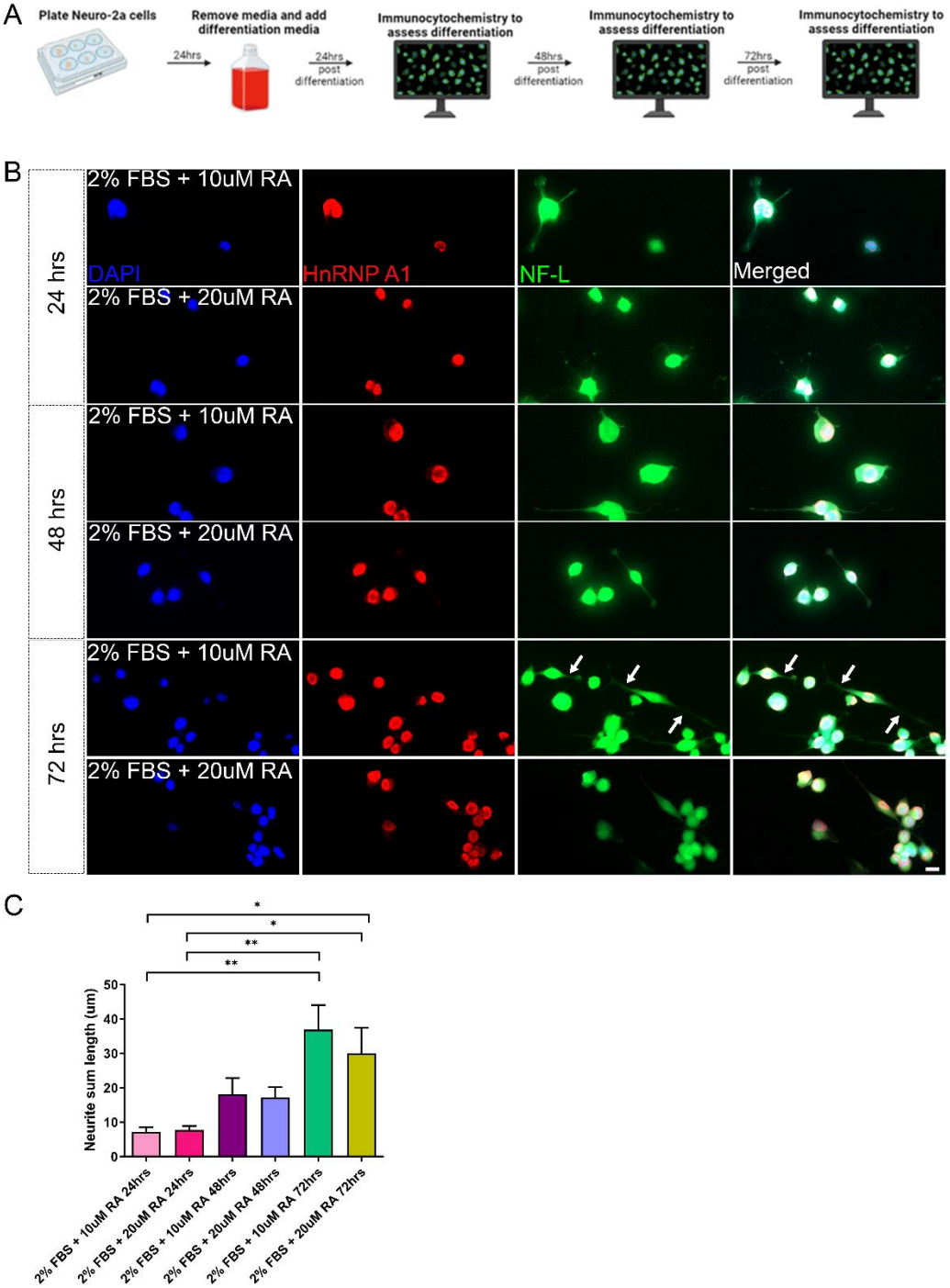

Figure 3.4 Differentiation of Neuro-2a cells in serum deprived media and RA. *A,* Neuro-2a differentiation and data collection protocol. *B,* Neuro-2a cells cultured in 2% FBS and 10µM or 20µm RA for 24 – 72 hours stained for DAPI (blue), hnRNP A1 (red) and NF-L (green). Arrows (white) indicate representative processes of differentiated Neuro-2a cells in the 2% FBS and 10µm RA for 72 hours condition. *C,* Quantification

revealed that Neuro-2a cells cultured in 2% FBS and 10µM or 20µM RA for 72 hours produced the longest processes. One-way ANOVA (*p<0.05, **p<0.01); n=10 cells per condition. Data are plotted as mean ± SEM.

3.1.3 Knockdown of hnRNP A1 in differentiated Neuro-2a cells

Next, to model loss-of-function of hnRNP A1, an optimized model of decreased hnRNP A1 protein expression in differentiated Neuro-2a cells needed to be established. For this purpose, Neuro-2a cells were differentiated for 72 hours in 2% FBS in combination with 10µM RA, after which siRNA transfections were performed for an additional 72 hours (Figure 3.5A). Figure 3.5B, C illustrate that knockdown of hnRNP A1 and cypB (positive control) was unsuccessful in differentiated Neuro-2a cells. However, this result was unsurprising considering that differentiated cells are known to have a low transfection efficiency and are considered difficult to transfect as compared to less differentiated or proliferating cells. Therefore, a new model was required to allow for successful knockdown of hnRNP A1 in differentiated Neuro-2a cells.

To allow for sufficient time of siRNA uptake in Neuro-2a cells, transfections were performed prior to differentiation (Figure 3.6A). In some cases, siRNA knockdown can be assessed as early as 4-24 hours after transfection[146]. Considering this, the 16-hour time point was chosen as a transfection window, to allow sufficient time for the siRNA to be taken up into the cell before media was changed to differentiation media. Neuro-2a cells were harvested at 16, 48 and 72 hours post siRNA transfection. Figures 3.6B, C demonstrate that even though the siRNA might be internalized into the cell by 16 hours, robust knockdown of hnRNP A1 is not apparent until 48 hours post transfection, with the 72 hours timepoint showing an even greater degree of hnRNP A1 knockdown. Considering this, the 72 hours timepoint was subsequently chosen for all downstream experiments evaluating consequences of loss-of-function of hnRNP A1. Further, to demonstrate loss of nuclear hnRNP A1, nuclear/cytoplasmic fractionation was performed, which confirmed a significant decrease in nuclear hnRNP A1 expression after 72 hours of siA1 treatment as compared to the control (Figure 3.6D, E).

To confirm uptake of siRNA at 16 hours post transfection, Neuro-2a cells were transfected with an AlexaFluor647 fluorescently tagged siA1 (siA1-AF647). Cells were

then fixed and immunostained for hnRNP A1 to visualize the fluorescently tagged siRNA. Figure 3.7A illustrates that at 16 hours post transfection, siA1-AF647 is taken up into the cell cytoplasm depicted by the pink punctate staining surrounding the nucleus (DAPI).

Additionally, knockdown of hnRNP A1 at 72 hours post siRNA transfection was confirmed through immunocytochemistry. Cells were fixed, immunostained for hnRNP A1, and quantified for hnRNP A1 nuclear fluorescence. Figure 3.8A, B demonstrate the quantitative difference in hnRNP A1 nuclear fluorescence in the siA1 treated group as compared to the control group. These results confirm successful hnRNP A1 knockdown in Neuro-2a cells 72 hours post siA1 treatment and validate its use as a model of loss-of-function of hnRNP A1.

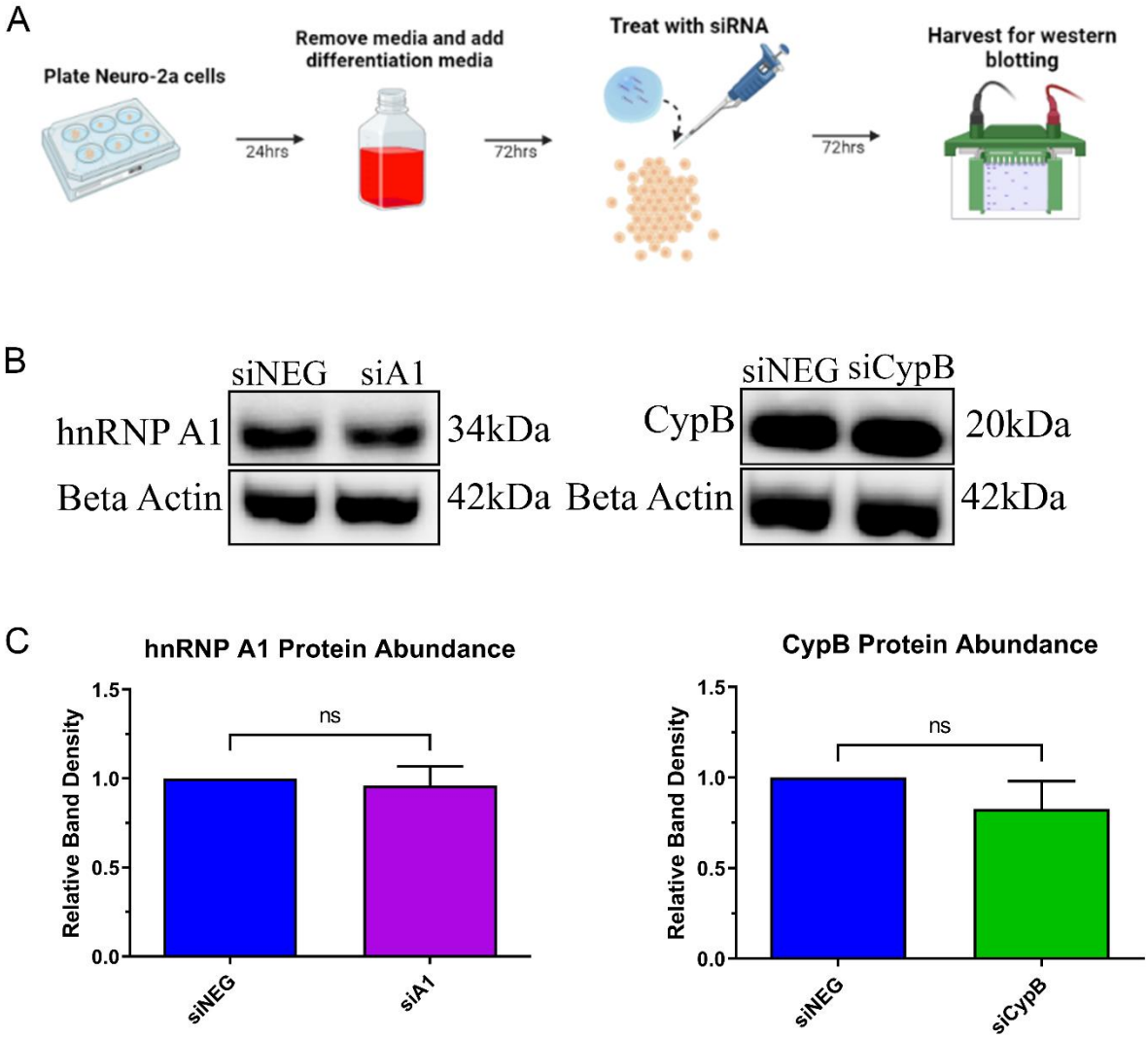

Figure 3.5 SiRNA knockdown is unsuccessful in 72 hours differentiated Neuro-2a cells. *A,* Neuro-2a differentiation, siRNA transfection and data collection protocol. *B,* Lysates from 72 hours differentiated Neuro-2a cells treated with siNEG or siA1 or siCypB for 72 hours were assayed by western blot for β-actin, hnRNP A1 and CypB. *C,* Band densitometry of western blots as in (B) demonstrates that there was no change in hnRNP A1 or CypB expression after siRNA transfection in differentiated Neuro-2a cells. Unpaired t-test (ns= not significant); n=3 biological replicates. Data are plotted as mean ± SEM.

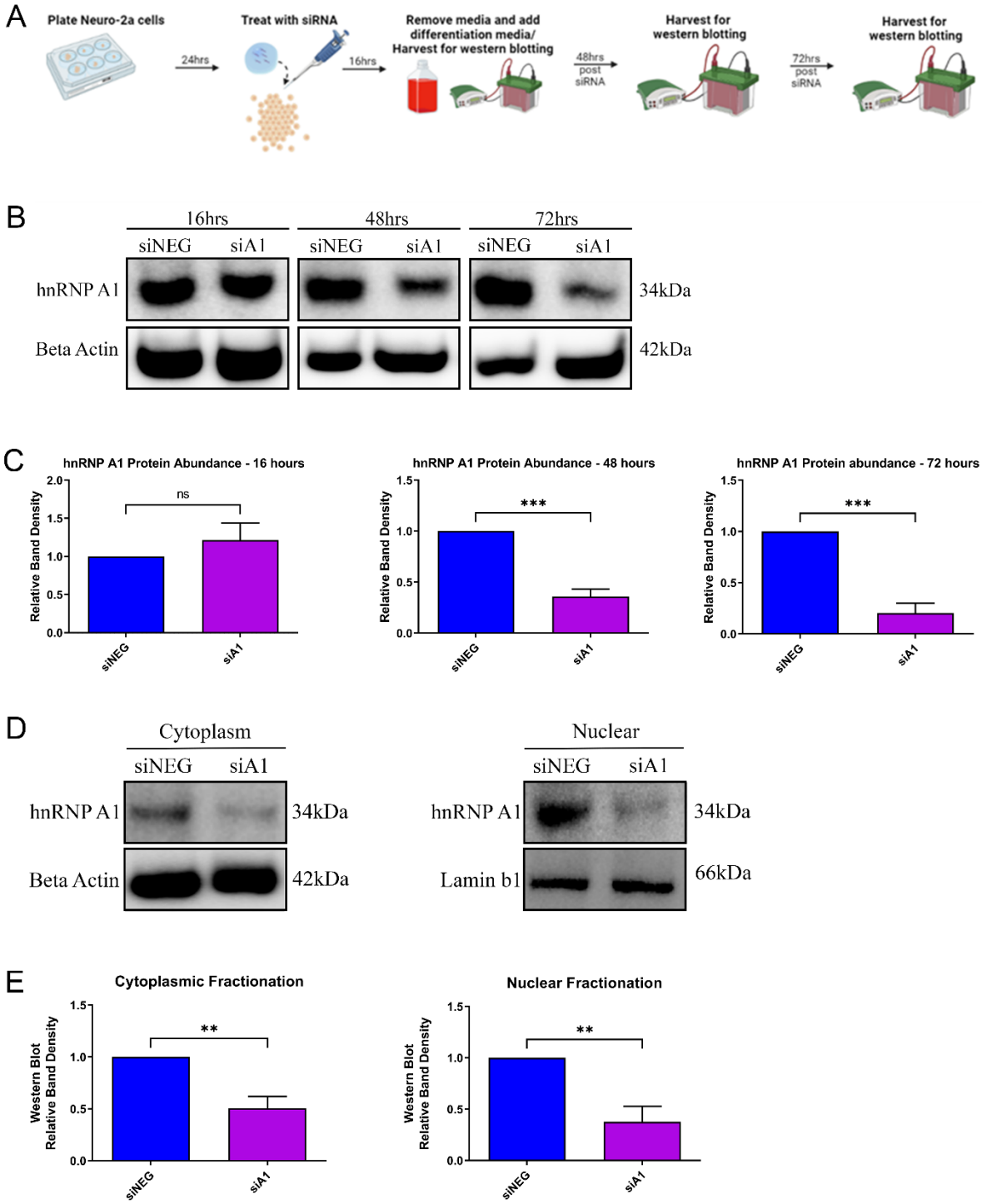

Figure 3.6 HnRNP A1 successfully knocked down at 72 hours post siA1 transfection. *A,* Neuro-2a cells siRNA transfection, differentiation and data collection protocol. *B,* Proteins from differentiated Neuro-2a cells treated with siNEG or siA1 for 16 – 72 hours were assayed by western blot for β-actin and hnRNP A1. *C,* Band densitometry

of western blots as in (B) demonstrates no change in hnRNP A1 protein expression at 16 hours post siA1, however a significant reduction in hnRNP A1 protein expression at 48 and 72 hours post siA1 as compared to siNEG treated cells. Unpaired t-test (ns=not significant, ***p<0.001); n=3 biological replicates. Data are plotted as mean ± SEM. *D,* Proteins from differentiated Neuro-2a cells treated with siNEG or siA1 for 72 hours were harvested for cytoplasmic and nuclear fractions and assayed by western blot. Cytoplasmic fractions were probed for β-actin and hnRNP A1. Nuclear fractions were probed for lamin b1 and hnRNP A1. *E,* Band densitometry of western blots as in (D) demonstrate significant reduction in nuclear hnRNP A1 protein expression at 72 hours post siA1 as compared to siNEG treated cells. Unpaired t-test (*p<0.05); n=3 biological replicates. Data are plotted as mean ± SEM.

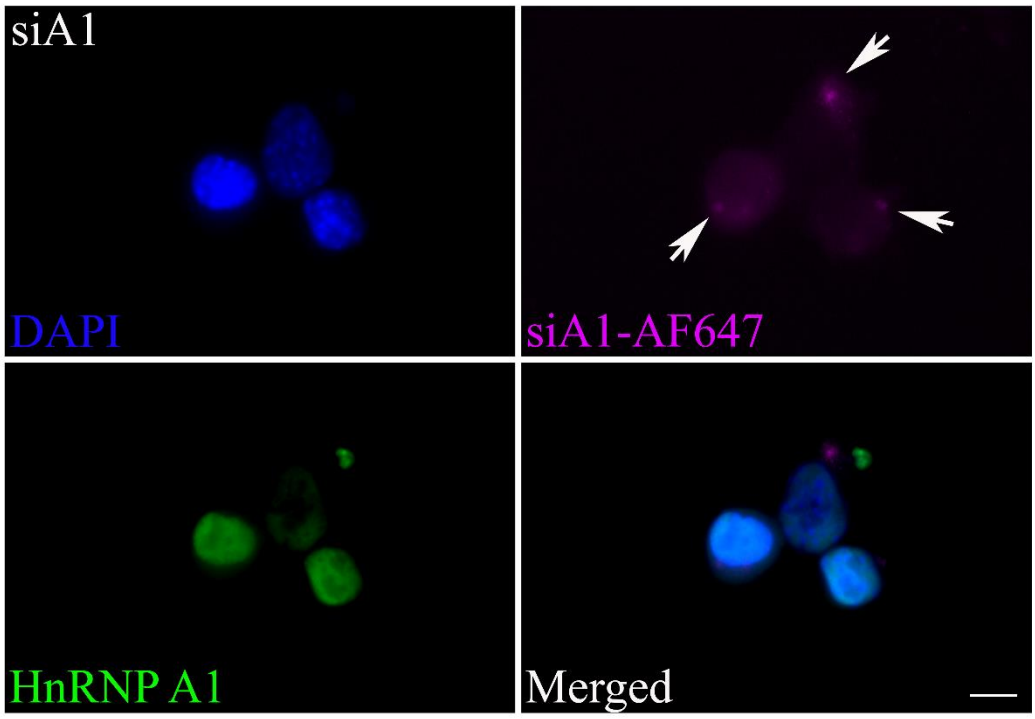

Figure 3.7 siRNA is internalized at 16 hours post siRNA transfection. Neuro-2a cells treated with siA1-AF647 for 16 hours and stained for DAPI (blue), hnRNP A1 (green). SiA1-AF647 (pink punctate staining) is present in the cytoplasm of Neuro-2a cells as indicated by arrows. Scale bar = 10μm.

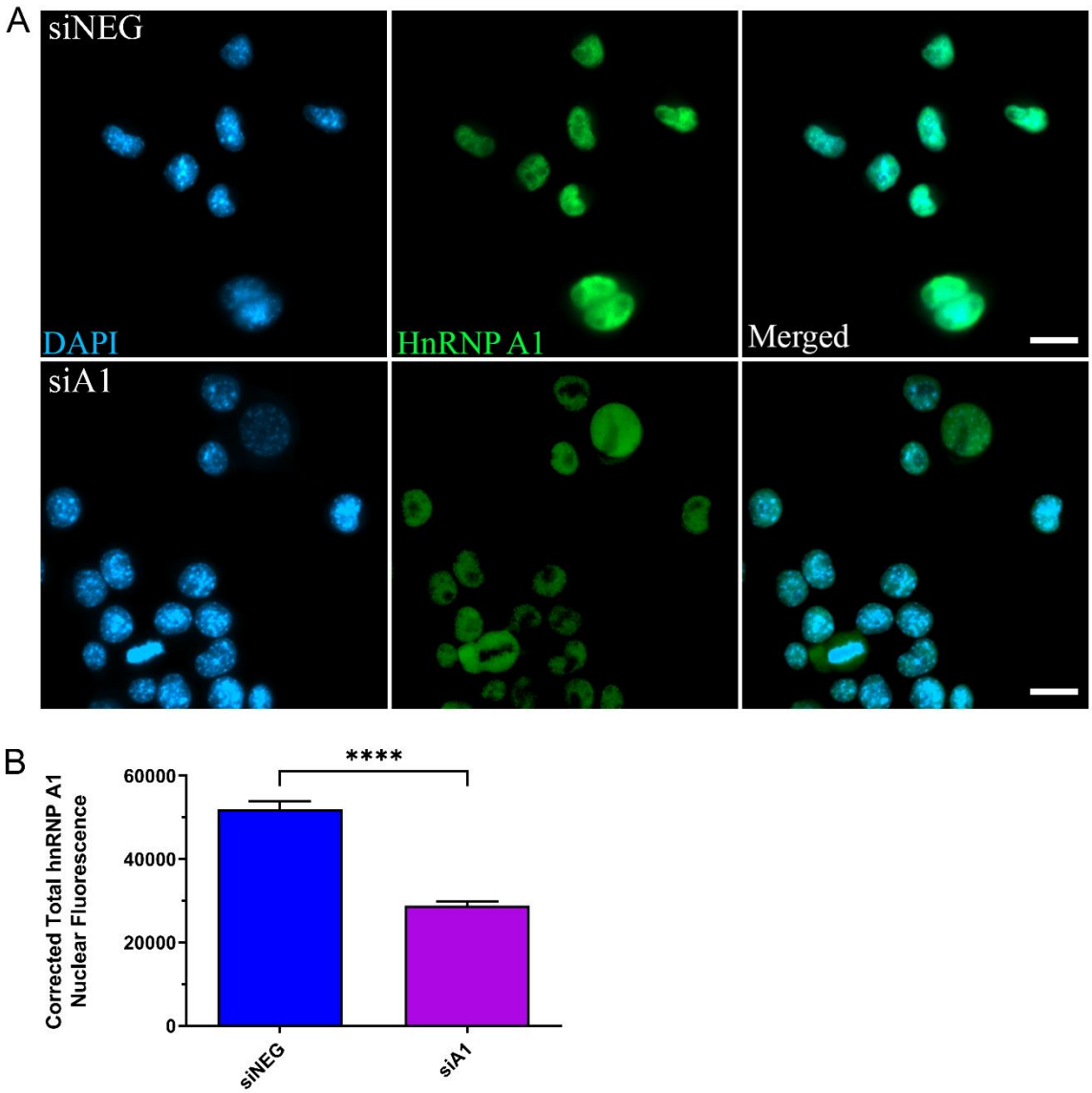

Figure 3.8 HnRNP A1 Knockdown is visualized at 72 hours post siA1 transfection. *A,* Differentiated Neuro-2a cells treated with siNEG or siA1 for 72 hours and stained for DAPI (blue) and hnRNP A1 (green). Scale bar = 50µm. *B,* Quantification of corrected total hnRNP A1 nuclear fluorescence revealed that cells in the siA1 treated condition have significantly lower hnRNP A1 nuclear fluorescence as compared to the siNEG condition. Unpaired t-test (****p< 0.0001); n=3 biological replicates; Individual cell values (n=30 cells per replicate) are plotted as mean ± SEM.

3.2 Effect of hnRNP A1 knockdown on RNA expression

Previous research in other neurodegenerative diseases have shown that dysfunctional RBPs result in wide scale RNA disturbances, which have been hypothesized to contribute to the pathogenesis of neurodegeneration[77–79]. To elucidate how loss-of-function of hnRNP A1, a form of RBP dysfunction observed in MS, affects RNA metabolism, RNAseq analysis followed by GO analysis was performed.

3.2.1 HnRNP A1 knockdown leads to dysregulation of transcripts involved in splicing, neuronal function, cell death and ribonucleoprotein complex formation

Neuro-2a cells treated with siNEG or siA1 according to the above established protocol were harvested for RNAseq analysis. Principal component analysis (PCA) revealed that the siNEG (n=3) and siA1 (n=3) samples formed distinct clusters with strong inter-cluster separation (Figure 3.9A). RNAseq analysis further revealed a total of 1,561 DE transcripts following hnRNP A1 knockdown (Figure 3.9B, C). Out of the 1,561 DE transcripts, 782 were significantly downregulated, and 779 were significantly upregulated. Additionally, our results revealed that hnrnpa1 was the most statistically significant gene between the siNEG and siA1 samples, which further supports the efficacy of the siRNA treatment (Figure 3.9C).

Next, to identify pathways and processes enriched from hnRNP A1 knockdown, GO analyses were performed. These analyses revealed that hnRNP A1 knockdown led to an enrichment of transcripts whose functions were related to RNA metabolism, including regulation of transcription, RNA splicing, RNA transport, and spliceosomal complex assembly (Figure 3.10A). Additionally, we found that hnRNP A1 knockdown led to an enrichment of transcripts related to neuronal functioning, including regulation of neurogenesis, nervous system development, and regulation of synapse structure or activity (Figure 3.10B). We also found an enrichment of transcripts whose functions were related to neurite outgrowth and cell death (Figure 3.10C, D), such as neuron projection development, regulation of axonogenesis, neuron projection maintenance, and regulation of programmed cell death. Lastly, we found an enrichment of transcripts whose functions were related to RNP complex assembly, which included RNP complex biogenesis, RNP

complex export from the nucleus, and regulation of protein complex disassembly (Figure 3.10E).

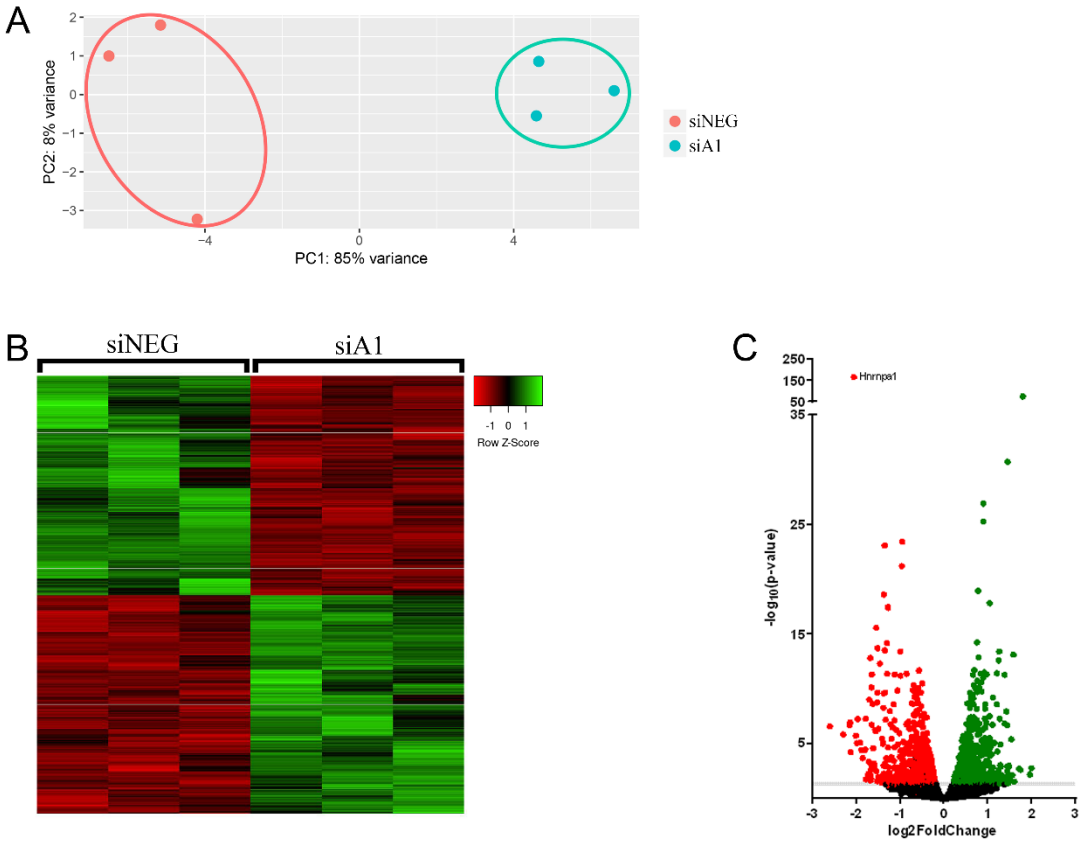

Figure 3.9 RNA-seq analysis of hnRNP A1 knockdown in differentiated Neuro-2a cells. *A,* PCA analysis of log transformed normalized RNAseq data showing that siA1 and siNEG formed distinct clusters with strong inter-cluster separation. *B,* Heatmap of DE transcripts plotted as normalized count values for siNEG (n=3) and siA1 (n=3) treated cells. *C,* Volcano plot of siA1 treated samples (siA1 vs siNEG) illustrating significantly upregulated (green dots) and downregulated (red dots) transcripts. Non-DE transcripts are represented as black dots. P threshold of 0.05 is displayed in grey.

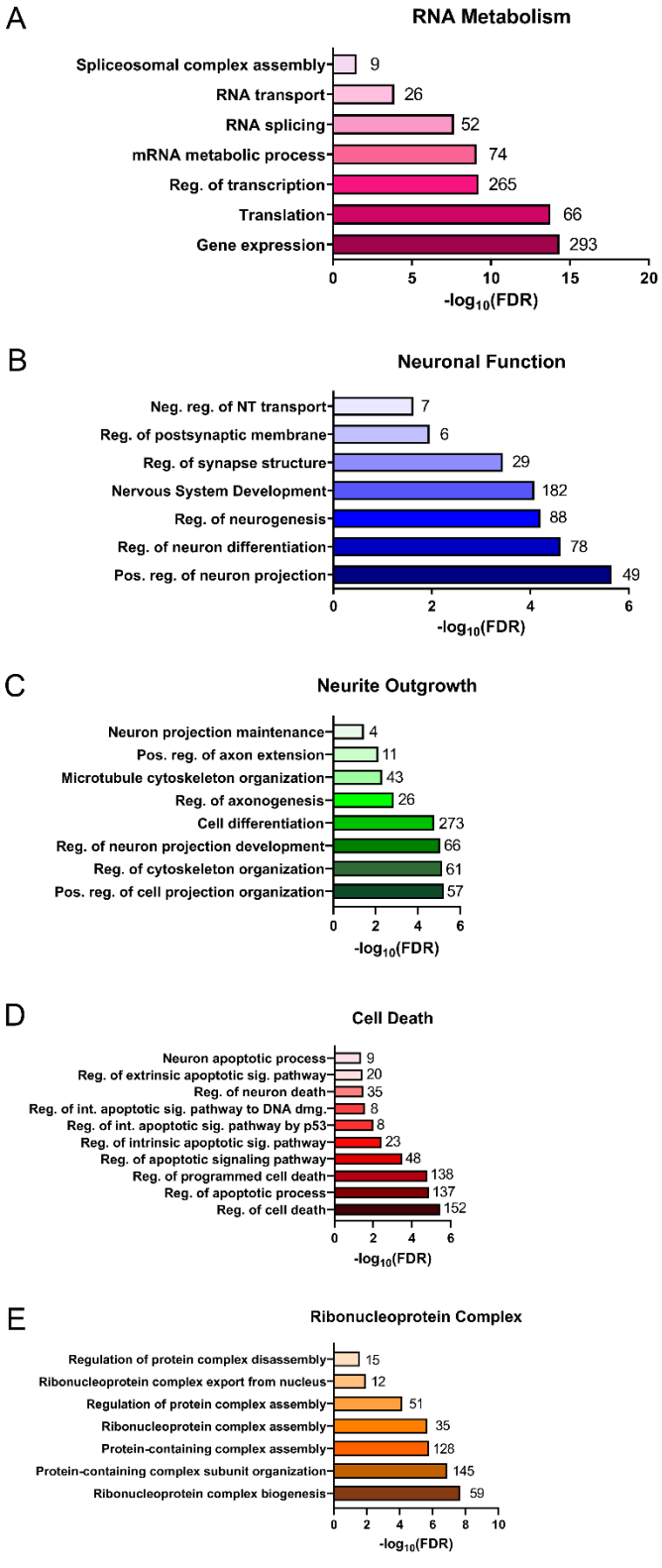

Figure 3.10 GO enrichment analysis of DE genes after hnRNP A1 knockdown in differentiated Neuro-2a cells. *A-E,* GO enrichment analysis of DE genes identified GO

terms related to RNA metabolism (A), neuronal function (B), neuronal morphology (C), cell death (D), and ribonucleoprotein complex (E). Values at the end of each bar represent number of DE genes in each GO process. Data are presented as -$\log_{10}$False discovery rate (FDR) values, which represent p-values adjusted for multiple tests by Benjamini-Hochberg procedure.

3.2.2 Majority of DE genes are known hnRNP A1 binding targets

Next, we investigated the relationship between our identified DE transcripts and transcripts that have been previously reported to bind to hnRNP A1. For this aim, we used Crosslinking ImmunoPrecipitation seq database (CLIPdb)[142], a public database with over 300 UV-crosslinking immunoprecipitation and sequencing datasets identifying transcripts that have shown to bind RBPs. Since there were no recorded datasets for transcripts shown to bind hnRNP A1 in mice, we converted our DE transcripts into human orthologs and overlaid our datasets with the available data from human studies showing hnRNP A1-bound transcripts. From our 1,561 DE mouse genes, 1,341 of those genes had human orthologs. We found that 1,204 out of the 1,342 DE genes (89.86%) had been previously found to bind hnRNP A1 (Figure 3.11A), with 88.89% of the upregulated genes (Figure 3.11B), compared to 91.9% of the downregulated genes (Figure 3.11C). These findings suggest that the majority of the identified DE transcripts might be dysregulated due to the inability of hnRNP A1 to bind these transcripts and properly process them.

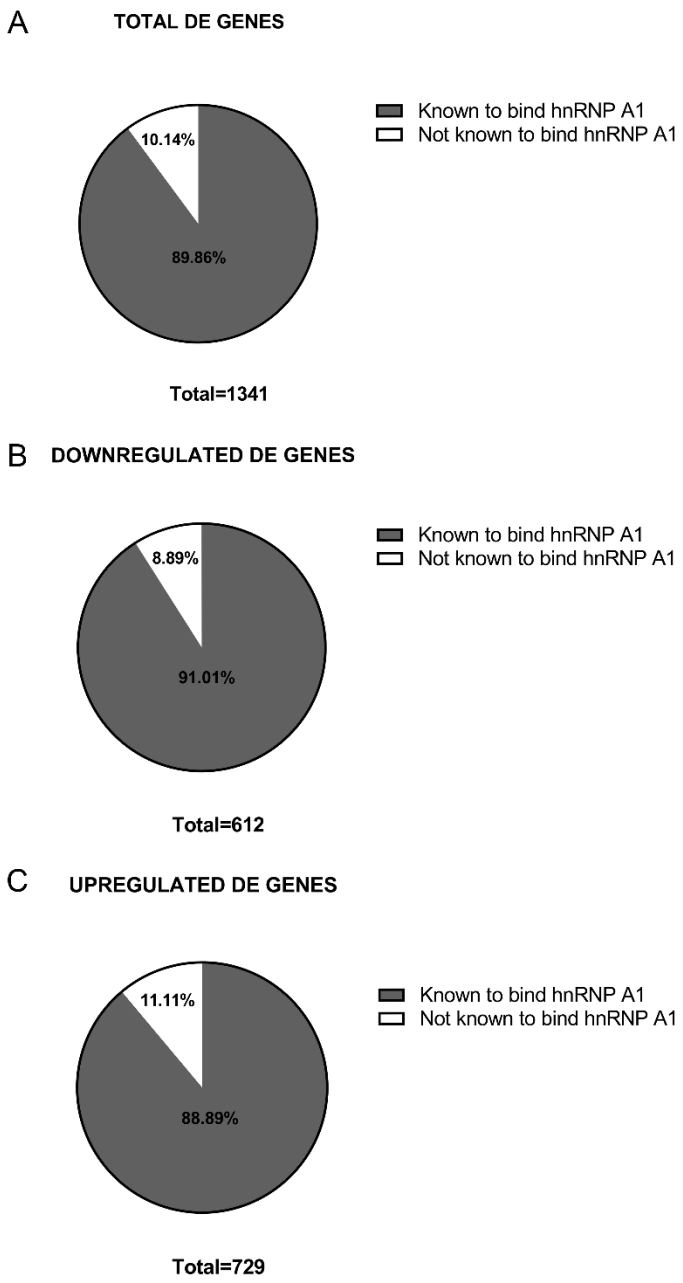

Figure 3.11 HnRNP A1 binding to DE genes. *A,* Pie chart representing the subset of DE genes with human orthologs (n=1,341) that had previously been shown to be known hnRNP A1 binding targets (89.86%) and those that had not (10.14%). *B,* Pie chart representing subset of upregulated DE genes with human orthologs (n=729) that had previously been shown to be known hnRNP A1 binding targets (88.89%) and those that had not (11.11%). *C,* Pie chart representing subset of downregulated DE genes with

human orthologs (n=612) that had previously been shown to be known hnRNP A1 binding targets (91.01%) and those that had not (8.89%).

3.3 Effect of hnRNP A1 knockdown on neuronal health, viability, and stress granule formation

Our RNA-seq analysis revealed enrichment of novel biological processes, such as neurite outgrowth, cellular death, and ribonucleoprotein complex formation, in the hnRNP A1 knockdown condition. To assess how hnRNP A1 knockdown affects each of these processes, additional downstream assays were performed.

3.3.1 Knockdown of hnRNP A1 negatively impacts neuronal morphology

The ability of differentiated neurons to grow their neurites in length and branching is an important morphological phenotype, which correlates with their function and health[147]. Our GO analyses revealed enrichment of DE genes for neurite outgrowth, therefore we sought to confirm this observation by assessing the effect of hnRNP A1 knockdown on neurite morphology. Neuro-2a cells treated with siNEG or siA1 following the previously established protocol were fixed and immunostained for hnRNP A1 and β-III-tubulin (Figure 3.12A). SiA1 treated Neuro-2a cells were first assessed for knockdown, which was quantitatively assessed as less than 50% hnRNP A1 fluorescence normalized to hnRNP A1 fluorescence in siNEG treated Neuro-2a cells. Neurite tracing quantification of these cells with hnRNP A1 knockdown revealed that siA1 treated Neuro-2a cells had significantly fewer neurite branches that were also shorter in length (Figure 3.12B, C). Further, we found a weak but statistically significant correlation between hnRNP A1 expression and neurite branching and neurite length (Figure 3.12C, E).

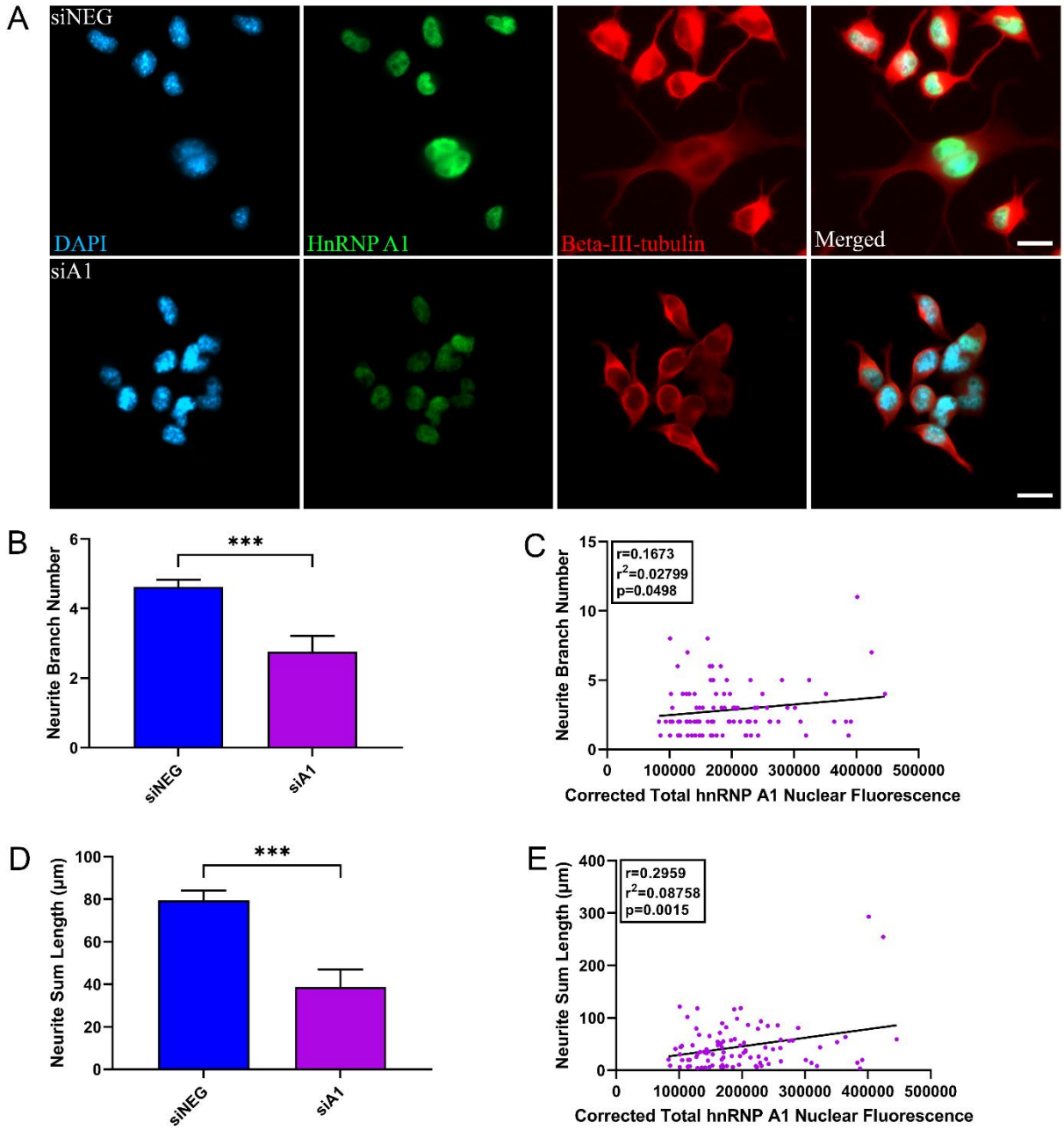

Figure 3.12 HnRNP A1 knockdown affects neuronal health. *A,* Differentiated Neuro-2a cells treated with siNEG or siA1 stained for DAPI (blue), hnRNP A1 (green) and β-III-tubulin (red) to identify neurites. Cells in the siNEG condition have more neurites that appear longer as compared to the siA1 condition. Scale bar = 20µm. *B,* Neurites were traced in the β-III-tubulin channel in ImageJ using the NeuronJ plugin as described in methods. Quantification revealed that siA1 treated cells have significantly fewer neurite branches as compared to the siNEG condition. Unpaired t-test (***p<0.001); n=3

biological replicates; n=30 cells per replicate for siNEG; n=20 cells with greater than 50% knockdown for siA1; Data are plotted as mean ± SEM. *C,* Corrected total hnRNP A1 nuclear fluorescence of Neuro-2a cells treated with siA1 correlates with neurite branch number. Pearson's correlation test (r=0.167, r^2=0.02799, p=0.0498); n=3 biological replicates; Individual cell values (n=30 cells per replicate) are plotted. *D,* Neuro-2a cells treated with siA1 have significantly shorter neurites as compared to the siNEG condition. Unpaired t-test (***p<0.001); n=3 biological replicates; n=30 cells per replicate for siNEG; n=20 cells with greater than 50% knockdown for siA1; Data are plotted as mean ± SEM. *E,* Corrected total hnRNP A1 nuclear fluorescence of Neuro-2a cells treated with siA1 correlated with neurite sum length. Pearson's correlation test (r=0.2959, r^2= 0.08758, p=0.0015); n=3 biological replicates; Individual cell values (n=30 cells per replicate) are plotted.

3.3.2 Knockdown of hnRNP A1 is detrimental to cell health

Next, we assessed whether siA1 treated Neuro-2a cells would display evidence of neuronal cell death. To assess hnRNP A1 knockdown affected levels of cytotoxicity, the LDH cytotoxicity assay was employed. We found that hnRNP A1 knockdown resulted in increased cytotoxicity as compared to cells treated with control (Figure 3.13A).

Our GO analyses revealed that among biological processes grouped under cell death, regulation of programmed cell death was among the processes that was highly enriched. To identify which form of cell death was activated, we explored apoptosis and necroptosis mediated cell death; two forms of programmed cell death pathways that have been robustly linked to neuronal cell death in MS[27–29]. Evidence of apoptosis mediated cell death was assessed through measuring the activity of caspase 3 and 7 through the Apo-ONE homogeneous caspase 3/7 assay. Figure 3.13B illustrates that hnRNP A1 knockdown in differentiated Neuro-2a cells did not significantly increase caspase 3/7 activity as compared to the control group.

Since our results indicated no evidence of apoptosis mediated cell death, we examined necroptosis mediated cell death. Neuro-2a cells were treated and differentiated according to the established protocol before being fixed and immunostained for β-III-tubulin, hnRNP A1 and pMLKL (a marker of necroptosis; Figure 3.13C). These results

demonstrated that Neuro-2a cells from the siA1 treated condition exhibited significantly greater number of cells with abnormal, punctate pMLKL staining as compared to the control condition (Figure 3.13D). The majority of the cells in the control condition displayed evenly dispersed and more diffuse pMLKL staining patterns, while siA1 treated cells exhibited significantly more peri-nuclear punctate like staining, indicative of the formation of a necrosome.

3.3.3 Decreased hnRNP A1 protein expression affects stress granule formation

Our GO term analysis revealed that RNP complex biogenesis was a biological process that was significantly enriched in our DE gene dataset. SGs are a form of RNP complex that assemble during stress and previous research has shown that hnRNP A1 is found in SGs under several stress conditions[98,103,148]. Therefore, to assess the role of hnRNP A1 in SGs, we examined how hnRNP A1 knockdown would affect SG formation and complexity. For this aim, Neuro-2a cells were treated with siRNA and differentiated according to the previously established protocol, after which SGs were induced using a classic stressor, sodium arsenite[133] (Figure 3.14A, B). Quantification revealed that hnRNP A1 knockdown significantly reduced the formation of SGs (Figure 3.14C), which correlated with hnRNP A1 expression (Figure 3.14D). Additionally, we found that the SGs that formed after hnRNP A1 knockdown were significantly reduced in size (Figure 3.14E). These results underscore the biologically important role of hnRNP A1 during the stress response and SG formation.

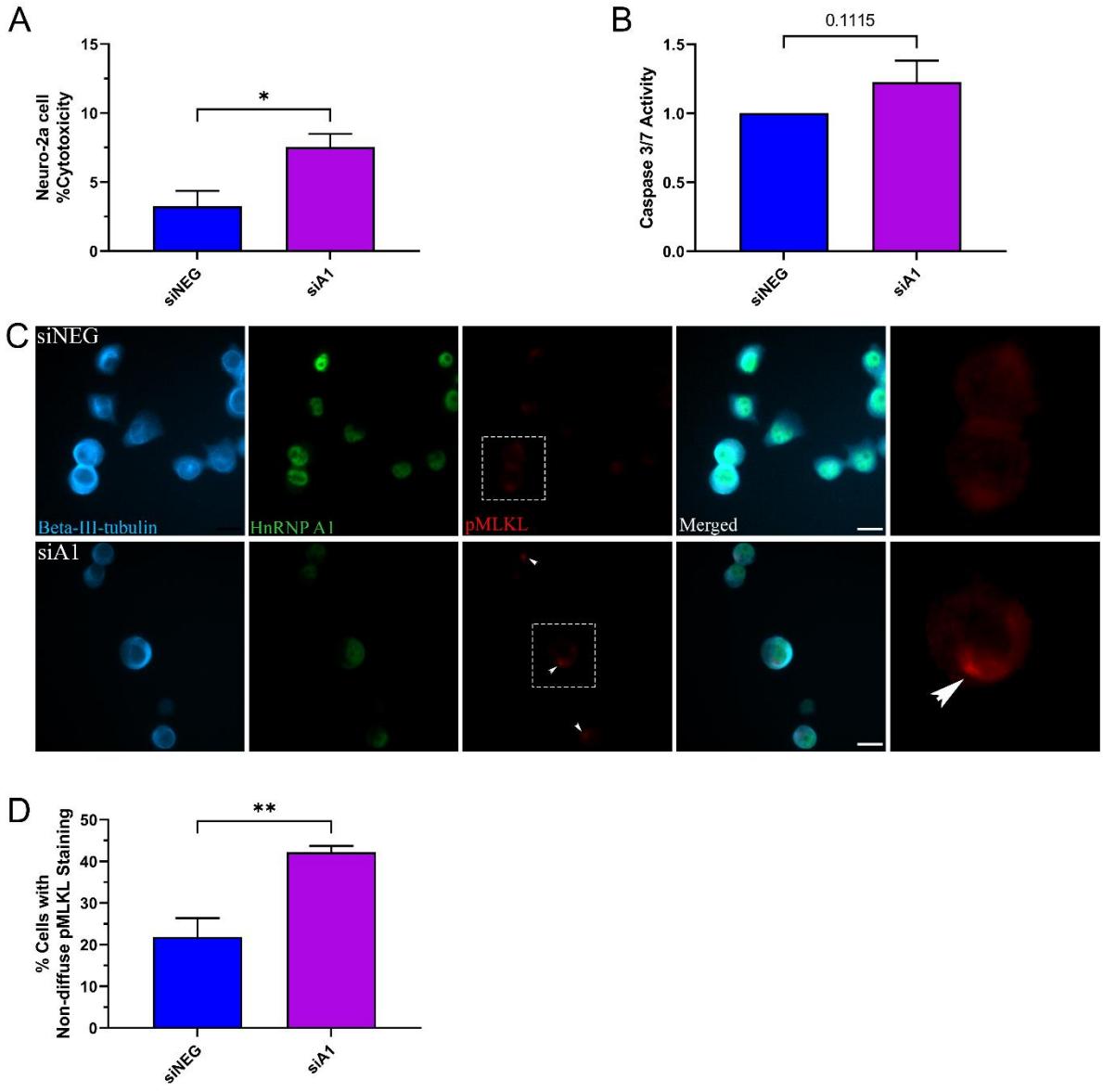

Figure 3.13 HnRNP A1 knockdown induces necroptosis mediated cell death. *A,* HnRNP A1 knockdown significantly increased cellular cytotoxicity as compared to siNEG treated cells, measured by the CYQUNAT LDH cytotoxicity assay. Unpaired t-test (*p<0.05); n=3 biological replicates; Data are plotted as mean ± SEM. *B,* HnRNP A1 knockdown resulted in no significant change in caspase 3/7 activity as compared to siNEG treated cells, measured through the apo-ONE homogeneous caspase 3/7 assay. Unpaired t-test (p=0.1115); n=3 biological replicates in triplicates; Data are plotted as mean ± SEM. *C,* Differentiated Neuro-2a cells treated with siNEG or siA1 stained for β-

III-tubulin (blue), hnRNP A1 (green) and pMLKL (red). Control cells exhibited diffuse pMLKL staining. Arrows indicate abnormal non-diffuse punctate staining in the siA1 treated condition. Scale bar = 20µm. *D,* Cells were qualitatively assessed for abnormal non-diffuse pMLKL staining in each condition. Quantification of this qualitative observation revealed that there was a significantly greater percentage of cells in the siA1 treated condition that exhibited non-diffuse pMLKL staining as compared to the siNEG condition. Unpaired t-test (**$p<0.01$); n=3 biological replicates with n=100 cells evaluated per replicate. Data are plotted as mean ± SEM.

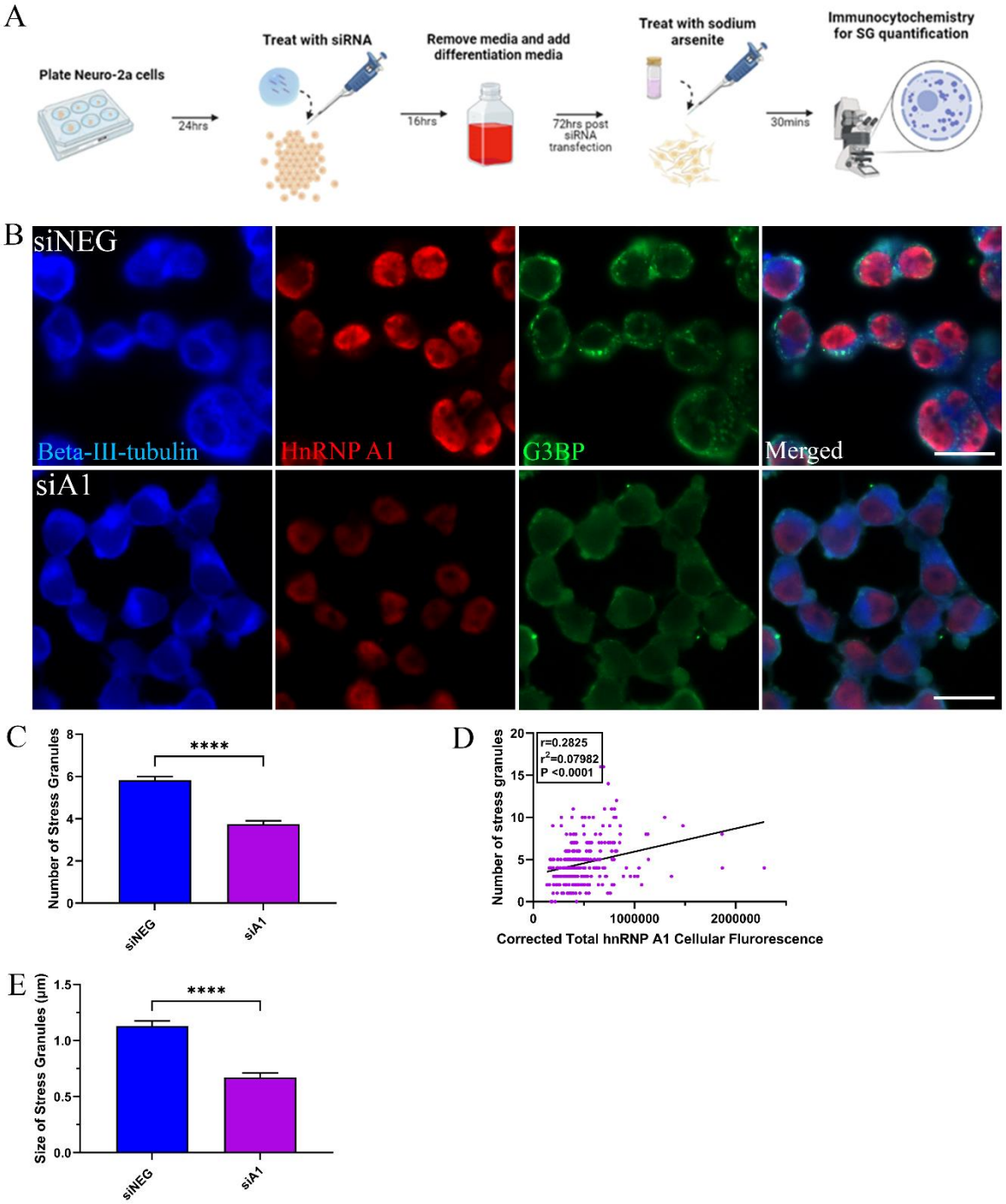

Figure 3.14 HnRNP A1 knockdown affects SG formation. *A,* Neuro-2a differentiation, siRNA treatment, sodium arsenite treatment and data collection protocol. *B,* Differentiated Neuro-2a cells treated with siNEG or siA1 followed by sodium arsenite treatment were stained for β-III-tubulin (blue), hnRNP A1 (red) and G3BP (green) to identify SGs. Cells in the siNEG condition have significantly more punctate-like G3BP^{+} granules as compared to the siA1 condition. Scale bar = 20µm. *C,* Quantification revealed that sodium

arsenite treated Neuro-2a cells in the siA1 condition form significantly fewer SGs as compared to the siNEG condition. Unpaired t-test (****p<0.0001); n=3 biological replicates; n=90 cells per replicate for siNEG; n=141 cells with greater than 50% knockdown for siA1; Data are plotted as mean ± SEM. *D,* HnRNP A1 cell fluorescence of Neuro-2a cells treated with siA1 followed by sodium arsenite treatment correlates with number of stress granules. Pearson's correlation test (r=0.2825, r^2= 0.07982, p<0.0001); n=3 biological replicates; Individual cell values (n=90 cells per replicate) are plotted. *E,* Quantification revealed that sodium arsenite treated Neuro-2a cells in the siA1 condition have significantly smaller SGs as compared to the siNEG condition. Unpaired t-test (****p<0.0001); n=3 biological replicates; n=90 cells per replicate for siNEG; n=141 cells with greater than 50% knockdown for siA1; Data are plotted as mean ± SEM.

CHAPTER 4: DISCUSSION

Dysfunction of RBPs, including hnRNP A1, have been shown to be key pathogenic features of neurodegenerative diseases such as ALS, FTLD and MS[90,92,108,110,149]. There are several hypotheses to explain the link between dysfunctional RBPs, specifically their mislocalization and loss of nuclear expression, and neurodegeneration. Two of the most common hypotheses include cytoplasmic gain-of-toxicity and nuclear loss-of-function[150,151]. The former suggests that there is a gain of toxicity in the cytoplasm when an RBP is mislocalized leading to consequences such as abnormal binding and processing of cytosolic RNA targets[79,152]. In the latter hypothesis, it is thought that RBP loss-of-function is deleterious leading to the lack of proper RNA processing, disrupted splicing regulation, and transcriptional control[153]. Data presented in this thesis presents novel insight into how loss-of-function of hnRNP A1 in a neuronal cell line may contribute to neuronal decline, which is highly relevant to MS pathogenesis.

4.1 Loss-of-function of hnRNP A1 can be modelled in differentiated Neuro-2a cells

First, to model loss-of-function of hnRNP A1, we employed the use of siRNA genetic knockdown. SiRNAs typically consist of 20-24 base RNA oligonucleotides that can be employed to interfere with the expression of a specific proteins[154]. Certain oligonucleotide sequences result in more potent knockdown in comparison to other sequences targeting the same RNA, which is largely owing to the complexity of the RNA interference pathway that the siRNAs employ. Therefore, it was pertinent to test different sequences of siRNAs that targeted hnRNP A1 to determine the most potent oligonucleotide sequence for hnRNP A1 knockdown. Transfection of these siRNA oligonucleotides into undifferentiated Neuro-2a cells revealed that siA1#4 was the most potent siRNA in knocking down hnRNP A1 (Figure 3.1), which was then chosen for all subsequent experiments and referred to as siA1.

Next, we wanted to establish a differentiation protocol for the Neuro-2a cells, which would exhibit distinct neuronal phenotypes, such as neurite branching and growth. Neuro-2a cells were chosen for our experiments due to their ability to easily differentiate into a neuron-like phenotype. However, research surrounding the reagents and conditions used to differentiate Neuro-2a cells was inconsistent. While some studies reported that serum

withdrawal or addition of factors such as cAMP, RA and NGF, were all capable of inducing differentiation[127,128], others proclaimed that these distinct conditions would produce morphologically distinct subtypes of neurons[126]. Therefore, we first tested two of the most frequently used differentiation conditions for Neuro-2a cells and defined our differentiation parameters as cells that produced the longest neurites. We were able to show that although ranges of serum withdrawal and addition of RA were able to differentiate Neuro-2a cells to a degree (Figure 3.2, 3.3), the differentiation condition that yielded the longest neurites was a combination of both serum withdrawal and RA (Figure 3.3), particularly when combining 2% FBS and 10µM of RA. Although this combinatorial condition produced differentiated Neuro-2a cells with the longest neurite lengths, research regarding the subtype of neurons this differentiation condition produces is largely limited.

Previous research comparing the use of neuronal cell lines versus primary neuronal cell culture, revealed that there were vast differences in the proteomic content and pathways related to neurodegenerative disease such as ALS[132]. Although this insight highlights the limitations for the use of a neuronal cell line for modelling disease, it is also important to note that differentiated neuronal cell lines, such as differentiated Neuro-2a cells, may possess more characteristics and proteomic similarities to primary cell culture, however this has yet to be thoroughly established.

The use of primary neuronal cell culture provides numerous benefits due to greater similarity to normal physiological conditions considering they are taken directly from the CNS. However, there are a myriad of hinderances in their use, which confer neuronal cell lines a better starting point for mechanistic studies. For example, primary neuronal cells exhibit a limited life span in comparison to neuronal cell lines and are also known to be difficult to transfect[155]. Additionally, primary cell cultures might also present a large degree of variability from culture to culture, conferring inconsistent results, especially for mechanistic studies. Although differentiated Neuro-2a cells may not be fully representative of the disease state or physiologic conditions, they can be a great asset and initial starting point for assessing experimental questions. This is underscored by several studies that have used differentiated neuronal cells and siRNA to model loss-of-

function of RBPs in the context of neurodegenerative diseases, which has led to identification of mechanistic pathways that can be verified in primary cells[129,156–158].

Similar to previous studies modelling loss-of-function of RBPs, we were able to establish a model for hnRNP A1 loss-of-function in differentiated Neuro-2a cells (Figure 3.6-3.8). Initial caveats to this endeavor were encountered when Neuro-2a cells were differentiated for 72 hours prior to transfection with siRNA. We showed that differentiation prior to transfection significantly affected the ability of cells to be transfected (Figure 3.5). Previous research has shown that siRNA uptake occurs between 4-16 hours post transfection[146], therefore, to overcome this issue, we decided to transfect our Neuro-2a cells 16 hours prior to differentiation. We showed that this paradigm of knockdown allowed sufficient uptake of the siRNA at the 16-hour timepoint, and that subsequent addition of differentiation media did not affect knockdown efficiency.

4.2 HnRNP A1 plays an important role in RNA expression

Following the establishment of a model of hnRNP A1 loss-of-function in differentiated Neuro-2a cells, we wanted to assess how loss of function would affect global RNA expression. For this purpose, we employed RNAseq followed by DE analysis, which revealed over 1,500 DE transcripts, with comparable numbers of upregulated and downregulated DE transcripts (Figure 3.9). Further, we were able to confirm that almost 90% of our DE genes had been previously shown to bind hnRNP A1 (Figure 3.11), suggesting that perturbations in the identified transcripts might be due to the lack of binding and proper processing by hnRNP A1. This result emphasized the highly integrated role of hnRNP A1 in many aspects of RNA metabolism and processing[93,95].

Our RNAseq results also validated our knockdown, whereby it confirmed that hnrnpa1 was the most significantly downregulated transcripts among all the DE transcripts. Interestingly, among the DE transcripts were tardbp and fus, which are transcripts that encode the RBPs, TDP-43 and FUS respectively, and have been previously linked to neurodegenerative diseases[159]. Moreover, hnRNP A1 has been previously shown to interact with TDP-43[160]. Our findings therefore suggest that hnRNP A1 function may influence the function of these other important RBPs, which together may contribute to the downstream deleterious consequences on neuronal health.

Next, we performed GO analysis using our identified DE transcripts to identify enriched biological processes after hnRNP A1 knockdown (Figure 3.10). Several enriched biological processes were related to RNA metabolism, including RNA splicing, regulation of transcription, and RNA transport, which are well established roles of hnRNP A1. For example, hnRNP A1 has been shown to regulate transcription through promoter activation[161] and suppression[162] of certain genes, such as controlling the degradation of inhibitory subunit of the nuclear factor κB (IκBα)[163], consequently resulting in the activation of nuclear factor κB (NF-κB), a transcriptional factor involved in regulating the immune response[164]. Furthermore, the role of hnRNP A1 in alternative splicing is well documented[94,98], including differential splicing of HIV-1 trans activator of transcription (HIV-Tat)[165]. While our data confirms a role for hnRNP A1 in these processes in neuronal cells, it also provides insight into RNA disturbances found in many neurodegenerative diseases, which might be linked to hnRNP A1 loss-of-function.

Given that neurons require tight homeostatic regulation of transcripts, large scale RNA disturbances, as observed in many neurological diseases, result in dire consequences on neuronal health. Dysregulation of RBPs, such as hnRNP A1, are often considered precipitating factors in these neurodegenerative diseases and contribute to the wide scale disruption in RNA metabolism within neurons. While literature suggests that hnRNP A1 is important in neuronal health, there have been no studies that have directly demonstrated this relationship. Our GO analyses revealed several enriched biological processes that were related to neuronal morphology, health, and development after hnRNP A1 knockdown, including axonogenesis, nervous system development, and regulation of neuron projection. Some of these terms establish an important role for hnRNP A1 in neuronal functioning, such as regulation of neuron projection, regulation of neurogenesis and regulation of neurotransmitter transport, while others, such as nervous system development, confirm previous findings[94,95,98,166]. For example, previous literature has demonstrated embryonic lethality in hnRNP A1 knockout mice, confirming the importance of hnRNP A1 in nervous system development[166]. However, the effects of hnRNP A1 knockdown on axonogenesis and neuron projection had yet to be thoroughly explored.

Death and damage to CNS resident cells such as neurons, oligodendrocytes and astrocytes is a well-established feature in MS pathogenesis[26–29]. A myriad of mechanisms such as the involvement of ROS, mitochondrial damage, autoimmunity and ongoing inflammatory infiltration have been proposed as leading culprits of cell death and damage while RBP dysfunction only recently being identified as a potential mechanism[9,18,31–33,36,50]. Therefore, until recently, little was known about how the dysfunction of RBPs may contribute to the cell death seen in MS tissue. Although many studies have now established dysfunctional RBPs, especially their loss-of-function as a prominent feature of MS neurons, none have mechanistically linked how loss-of-function of hnRNP A1 may result in cell death. Our GO analysis revealed that hnRNP A1 knockdown resulted in an enrichment of transcripts related to cell death, which includes regulation of neuron death and regulation of programmed cell death. These results provide novel insight into an RBP-based mechanism of neurodegeneration in MS.

Finally, our GO analysis revealed an enrichment for the biological process RNP complex assembly. Intriguingly, SGs, an RNP complex, are a feature of dysfunctional RBPs in disease and are often found to be colocalized with mislocalized RBPs in the cytoplasm of cells[118]. Therefore, our results confirm the biologically important role of hnRNP A1 in the assembly of RNP complexes in neuronal cells. However, how the loss-of-function of hnRNP A1 may disrupt the formation of SGs during a stress response in neuronal cells had not been explored.

4.3 Loss-of-function of hnRNP A1 results in deleterious consequences for neuronal health

Our GO analyses revealed a subset of novel enriched biological processes that had not been thoroughly explored in the context of loss-of-function of hnRNP A1 in neurodegenerative diseases. To validate these findings and determine whether hnRNP A1 knockdown specifically affects neurite outgrowth, cell viability and SG formation after stress, we performed further experimental assays. Previous studies have shown that hnRNP A1 may play an indispensable role in cellular biology, since the expression of other functionally similar RBPs were unable to compensate for the loss-of-function of hnRNP A1[166]. Considering this, we hypothesized that hnRNP A1 knockdown would have

negative consequences on neurite outgrowth, cell viability as well as on the formation and complexity of SGs.

First, to assess the effect of hnRNP A1 loss-of-function on neurite outgrowth, we examined neurite branching and neurite length following hnRNP A1 knockdown. Our results revealed that hnRNP A1 knockdown decreased the branching and length of neurites as compared to the control treated group. Additionally, neurite length and branching were found to positively correlate with hnRNP A1 nuclear expression in hnRNP A1 knockdown cells (Figure 3.12). These results demonstrate that hnRNP A1 plays an active role in neurite outgrowth; however, the exact mechanism by which this occurs remains to be elucidated. One possibility is that hnRNP A1 regulates transcripts important for these processes. For example, TDP-43 has been shown to be involved in the regulation of Rho family GTPases[129] and histone deacetylases[158], key components for neurite outgrowth in neuronal cells. A similar mechanism may be employed by hnRNP A1. Furthermore, hnRNP A1 has been shown to interact with TDP-43[160], which suggests hnRNP A1 may secondarily affect neurite outgrowth by affecting the functions that TDP-43 has on neurite outgrowth proteins.

Next, to validate our GO analysis on the enrichment of cellular death biological processes and to assess whether hnRNP A1 loss-of-function results in neuronal cell death, we chose to assess the degree of cell death using a LDH cytotoxicity assay. Previously, a study examining the effect of loss-of-function of TDP-43 in differentiated Neuro-2a cells revealed that TDP-43 knockdown significantly increased cell death and decreased viability[129]. Our results showed that like TDP-43, knockdown of hnRNP A1 in differentiated Neuro-2a cells increased cell cytotoxicity (Figure 3.13). These results provide novel insight into the biologically important role of hnRNP A1 in neuronal cell health and viability.

Following this initial observation, we wanted to delineate the mechanism by which cell death was occurring. Pathological findings in MS tissue have suggested a role for both apoptosis[27] and necroptosis[28,29] as mechanisms of neuron death. Therefore, we chose to explore these two forms of cell death after hnRNP A1 knockdown. Our results revealed that cell death after hnRNP A1 loss-off-function was not mediated through

apoptosis, evidenced by the lack of increase in effector caspases activity (Figure 3.13). However, when immunostaining for pMLKL, a marker of necroptosis, we observed distinct differences in staining patterns between the siA1 and siNEG treated conditions. We showed that control conditions had a higher percentage of cells with diffuse pMLKL staining, indicative of normal pMLKL staining with no necrosome formation, while cells with hnRNP A1 knockdown exhibited more punctate staining of pMLKL (Figure 3.13). In the activation of necroptosis, pMLKL is known to form a core component of the protein oligomer known as a necrosome, which is often visualized as a punctate within the cells undergoing necroptosis. Considering this, it may be possible that hnRNP A1 loss-of-function triggers intracellular dysfunction that culminates in the formation of $pMLKL^{+}$ necrosomes, resulting in cell death. Although previous findings have largely alluded to inflammatory infiltrates as the key players in triggering cascades of cell death, our data sheds novel insight that RBP dysfunction, by means of decreased hnRNP A1 expression, may contribute to the cascade of neuronal death that is observed in MS.

Lastly, we wanted to examine the effect of decreased hnRNP A1 protein expression on the formation of SGs after induction of sodium arsenite stress. SGs typically form during stress and are of biological importance as they harbor translationally stalled RNAs throughout the duration of the stressor to preserve cellular energy[167]. HnRNP A1 has been shown to associate with SGs under stress conditions and co-localize with SGs under pathologic conditions[110,117,118]. Our results revealed that hnRNP A1 knockdown significantly reduced both the number of SGs and the size of SGs that formed. Additionally, both number of SGs and size were seen to positively correlate with hnRNP A1 cellular fluorescence in the siA1 treated condition (Figure 3.14). These results suggest that hnRNP A1 either directly or indirectly influences SGs kinetics during stress. One possibility is that since hnRNP A1 plays a vital role in regulating RNA metabolism, it might be involved in transporting RNAs into SGs or regulate other RBPs that actively regulate SG formation. These findings align with previous studies showing that hnRNP A1 associates with SGs in HeLa cells and that knockdown of hnRNP A1 impacts the cell's ability to recover from stress[117].

CHAPTER 5: CONCLUSION AND FUTURE DIRECTIONS

MS is a chronic autoimmune demyelinating disease of the CNS, with a profound neurodegenerative component, whereby there is death and damage to neurons. Robust research has now demonstrated that neurodegeneration starts early in disease and that the degree of neurodegeneration directly correlates with permanent disability[13,19–22]. Current disease modifying therapies in MS have been inadequate in modulating the neurodegenerative component of disease and this is largely due to the lack of mechanistic insight into the true drivers of the pathogenesis of neurodegeneration in MS.

Many studies have now linked dysfunctional RBPs as key drivers of neurodegeneration in many other neurodegenerative diseases such as ALS, FTLD and AD. More recently, the contribution of dysfunctional RBPs has been explored in MS, whereby similar features of RBP dysfunction were observed in MS neurons. Neurons from MS brains revealed a continuum of nuclear-cytoplasmic mislocalization of hnRNP A1, resulting in increased hnRNP A1 in the cytoplasm and complete nuclear depletion of hnRNP A1, a severe RBP dysfunction phenotype[109,110]. These dysfunctional features were additionally observed in the EAE animal model of MS and were shown to correlate with neuronal death and markers of neurodegeneration[78,108]. These initial findings spurred the debate into whether hnRNP A1 gain-of-toxicity in the cytoplasm or loss-of-function in the nucleus were the main drivers of dysfunction and neurodegeneration. Here, we provide evidence that loss-of-function of hnRNP A1, as seen in MS neurons through mislocalization and nuclear depletion, results in devastating consequences on RNA expression, neuronal health, viability and perturbs the formation of SGs during stress.

First, we set out to model loss-of-function of hnRNP A1 using siRNA and differentiated neuronal cell line. We showed successful knockdown of hnRNP A1 in differentiated Neuro-2a cells. Although neuronal cell lines, especially once differentiated, can generate valuable insight into mechanistic questions, they are predominantly limited in their ability to simulate a physiological state and model the complexities of disease. Future studies should, therefore, investigate the role of loss-of-function of hnRNP A1 in primary neuronal cells, as well as *in vivo* in animal models to provide greater relevance to human disease. It is well known that there is significant damage to oligodendrocytes in

MS, and more recently, it has been revealed that oligodendrocytes also exhibit dysfunctional features of RBPs, more specifically reduced expression, in MS tissue[92]. Additional future studies could, therefore, benefit from investigating the role that loss-of-function of these RBPs play in their deterioration.

Next, we examined the effect of hnRNP A1 loss-of-function on total RNA expression and found that there were over 1,500 DE transcripts in the hnRNP A1 knockdown condition, over 90% had been previously shown to bind hnRNP A1. These findings demonstrated that hnRNP A1 knockdown may be directly related to hnRNP A1's diminished binding and processing of the DE transcripts. Further, our GO analysis revealed an enrichment of biological processes that were related to RNA metabolism, neuronal health, neurite outgrowth, cellular death and RNP complex formation. While some of these biological processes confirmed previously established roles of hnRNP A1 such as its integral role in alternative splicing and processing, others provided novel insight into hnRNP A1's role in controlling neuronal neurite outgrowth and neuronal death. Our RNAseq and GO analysis findings can be utilized as a database, which include all DE transcripts and enriched biological processes. Given this, future studies could examine specific pathways that might be disrupted after hnRNP A1 knockdown to uncover mechanistic insights into how each biological process is affected.

To elucidate how hnRNP A1 knockdown affected each biological process uncovered from our GO analysis, we first examined neurite outgrowth. Our results demonstrated that hnRNP A1 knockdown decreased both neurite length and branching, both of which correlated with hnRNP A1 nuclear expression in the siA1 condition. Although these results demonstrate a direct relationship between hnRNP A1 knockdown and neurite outgrowth, little is known regarding the pathways that lead to this change. Therefore, future studies should examine specific differentially expressed transcripts that may be involved in this process to offer mechanistic insight.

When examining the effects of hnRNP A1 knockdown on neuronal cell death, our results revealed that hnRNP A1 knockdown resulted in a significant increase in cell cytotoxicity. Further, we showed that there was no significant difference in the caspase 3/7 activity between hnRNP A1 knockdown and control conditions suggesting that cell

death was not apoptosis mediated. Rather, our results alluded to the involvement of the necroptotic cell death pathway, owing to our observation that cells treated with siA1 exhibited punctate pMLKL staining, indicative of formation of necrosomes. Considering the recently established presence of necroptotic cell death in MS tissue, future studies should thoroughly explore the link between dysfunctional RBPs and activation of necroptosis.

Lastly, we examined the effects of hnRNP A1 knockdown on the formation of SGs and their complexity. Previous research has shown that hnRNP A1 interacts with SGs during the stress response, however, little is known about hnRNP A1's role in SG formation. Our results, therefore, also provide novel insight into hnRNP A1's integral role in the formation of SGs. However, future studies should investigate the proteomic contents of the SGs formed after hnRNP A1 to further elucidate the key players leading to these changes.

Elucidating how loss-of-function of hnRNP A1 in neuronal cells impacts neuronal health, viability and SG formation provides mechanistic insight into how dysfunctional hnRNP A1, particularly decreased hnRNP A1 expression, in MS neurons may contribute to the pathogenesis of neurodegeneration. Further, these findings could aid in the development of novel therapies targeting hnRNP A1 dysfunction that inhibit, halt or reverse neurodegeneration and its associated disabilities in MS.

CHAPTER 6: REFERENCES

1. Anees, A. *et al.* Knockdown of heterogeneous nuclear ribonucleoprotein A1 results in neurite damage, altered stress granule biology and cellular toxicity in differentiated neuronal cells. *eNeuro* ENEURO.0350-21.2021 (2021) doi:10.1523/ENEURO.0350-21.2021.
2. Oh, J., Vidal-Jordana, A. & Montalban, X. Multiple sclerosis: Clinical aspects. *Curr. Opin. Neurol.* **31**, 752–759 (2018).
3. Charcot, J.-M. (1825-1893). Histologie de la sclérose en plaques, leçon faite à l'hospice de la Salpêtrière par M. Charcot et recueillie par M. Bourneville. *Gaz Hop* **41**, 554–5 557–8 (1869).
4. Dawson, J. W. XVIII.—The histology of disseminated sclerosis. *Trans. R. Soc. Edinburgh* **50**, 517–740 (1916).
5. Reich, D. S., Lucchinetti, C. F. & Calabresi, P. A. Multiple Sclerosis. *N. Engl. J. Med.* **378**, 169 (2018).
6. Polman, C. H. *et al.* Diagnostic criteria for multiple sclerosis: 2010 Revisions to the McDonald criteria. *Ann. Neurol.* **69**, 292 (2011).
7. Thompson, A. J. *et al.* Diagnosis of multiple sclerosis: 2017 revisions of the McDonald criteria. *Lancet Neurol.* **17**, 162–173 (2018).
8. Trapp, B. D. & Nave, K. A. Multiple sclerosis: An immune or neurodegenerative disorder? *Annu. Rev. Neurosci.* **31**, 247–269 (2008).
9. JH, N., C, L., M, R. & BG, W. Multiple sclerosis. *N. Engl. J. Med.* **343**, 938–952 (2000).
10. Levin, M. *et al.* Pathogenic mechanisms of neurodegeneration based on the phenotypic expression of progressive forms of immune-mediated neurologic disease. *Degener. Neurol. Neuromuscul. Dis.* **2**, 175 (2012).
11. Lassmann, H., Brück, W. & Lucchinetti, C. F. The immunopathology of multiple sclerosis: An overview. *Brain Pathol.* **17**, 210–218 (2007).
12. Compston, A. & Coles, A. Multiple sclerosis. *Lancet* **372**, 1502–1517 (2008).
13. Trapp, B. D. *et al.* Axonal Transection in the Lesions of Multiple Sclerosis. *N. Engl. J. Med.* **338**, 278–285 (1998).
14. Coles, A. J. *et al.* The window of therapeutic opportunity in multiple sclerosis:

Evidence from monoclonal antibody therapy. *J. Neurol.* **253**, 98–108 (2006).

15. Frischer, J. M. *et al.* The relation between inflammation and neurodegeneration in multiple sclerosis brains. *Brain* **132**, 1175–1189 (2009).
16. Miller, D. H., Barkhof, F., Frank, J. A., Parker, G. J. M. & Thompson, A. J. Measurement of atrophy in multiple sclerosis: Pathological basis, methodological aspects and clinical relevance. *Brain* **125**, 1676–1695 (2002).
17. Kutzelnigg, A. *et al.* Cortical demyelination and diffuse white matter injury in multiple sclerosis. *Brain* **128**, 2705–2712 (2005).
18. Friese, M. A., Schattling, B. & Fugger, L. Mechanisms of neurodegeneration and axonal dysfunction in multiple sclerosis. *Nat. Rev. Neurol.* **10**, 225–238 (2014).
19. Barnes, D., Munro, P. M. G., Youl, B. D., Prineas, J. W. & Mcdonald, W. I. The longstanding ms lesion. *Brain* **114**, 1271–1280 (1991).
20. Davie, C. A. *et al.* Persistent functional deficit in multiple sclerosis and autosomal dominant cerebellar ataxia is associated with axon loss. *Brain* **118**, 1583–1592 (1995).
21. Kidd, D. *et al.* Spinal cord mri using multi-array coils and fast spin echo: Ii. findings in multiple sclerosis. *Neurology* **43**, 2632–2637 (1993).
22. Losseff, N. A. *et al.* Spinal cord atrophy and disability in multiple sclerosis. A new reproducible and sensitive MRI method with potential to monitor disease progression. *Brain* **119**, 701–708 (1996).
23. Ferguson, B., Matyszak, M. K., Esiri, M. M. & Perry, V. H. Axonal damage in acute multiple sclerosis lesions. *Brain* **120**, 393–399 (1997).
24. Kornek, B. *et al.* Multiple sclerosis and chronic autoimmune encephalomyelitis: A comparative quantitative study of axonal injury in active, inactive, and remyelinated lesions. *Am. J. Pathol.* **157**, 267–276 (2000).
25. Fink, S. L. & Cookson, B. T. Apoptosis, pyroptosis, and necrosis: Mechanistic description of dead and dying eukaryotic cells. *Infect. Immun.* **73**, 1907–1916 (2005).
26. M. Reichardt, H. & Luhder, F. The Ambivalent Role of Apoptosis in Experimental Autoimmune Encephalomyelitis and Multiple Sclerosis. *Curr. Pharm. Des.* **18**, 4453–4464 (2012).

27. Hisahara, S. *et al.* Targeted expression of baculovirus p35 caspase inhibitor in oligodendrocytes protects mice against autoimmune-mediated demyelination. *EMBO J.* **19**, 341–348 (2000).
28. Picon, C. *et al.* Neuron-specific activation of necroptosis signaling in multiple sclerosis cortical grey matter. *Acta Neuropathol.* **141**, 585–604 (2021).
29. Ofengeim, D. *et al.* Activation of necroptosis in multiple sclerosis. *Cell Rep.* **10**, 1836–1849 (2015).
30. Constantinescu, C. S., Farooqi, N., O'Brien, K. & Gran, B. Experimental autoimmune encephalomyelitis (EAE) as a model for multiple sclerosis (MS). *Br. J. Pharmacol.* **164**, 1079–1106 (2011).
31. Nikić, I. *et al.* A reversible form of axon damage in experimental autoimmune encephalomyelitis and multiple sclerosis. *Nat. Med.* **17**, 495–499 (2011).
32. Zeis, T. *et al.* Molecular changes in white matter adjacent to an active demyelinating lesion in early multiple sclerosis: Molecular changes in MS periplaque white matter. *Brain Pathol.* **19**, 459–466 (2009).
33. Haider, L. *et al.* Oxidative damage in multiple sclerosis lesions. *Brain* **134**, 1914–1924 (2011).
34. Trapp, B. D. & Stys, P. K. Virtual hypoxia and chronic necrosis of demyelinated axons in multiple sclerosis. *Lancet Neurol.* **8**, 280–291 (2009).
35. Campbell, G. R. *et al.* Mitochondrial DNA deletions and neurodegeneration in multiple sclerosis. *Ann. Neurol.* **69**, 481–492 (2011).
36. Forte, M. *et al.* Cyclophilin D inactivation protects axons in experimental autoimmune encephalomyelitis, an animal model of multiple sclerosis. *Proc. Natl. Acad. Sci. U. S. A.* **104**, 7558–7563 (2007).
37. Kinnally, K. W., Peixoto, P. M., Ryu, S. Y. & Dejean, L. M. Is mPTP the gatekeeper for necrosis, apoptosis, or both? *Biochim. Biophys. Acta - Mol. Cell Res.* **1813**, 616–622 (2011).
38. Millecamps, S. & Julien, J. P. Axonal transport deficits and neurodegenerative diseases. *Nat. Rev. Neurosci.* **14**, 161–176 (2013).
39. Hirokawa, N., Niwa, S. & Tanaka, Y. Molecular motors in neurons: Transport mechanisms and roles in brain function, development, and disease. *Neuron* **68**,

610–638 (2010).

40. McCauley, J. L. & Hussman, J. P. Comprehensive follow-up of the first genome-wide association study of multiple sclerosis identifies KIF21B and TMEM39A as susceptibility loci. *Hum. Mol. Genet.* **19**, 953–962 (2010).
41. Hares, K. *et al.* Axonal motor protein KIF5A and associated cargo deficits in multiple sclerosis lesional and normal-appearing white matter. *Neuropathol. Appl. Neurobiol.* **43**, 227–241 (2017).
42. Kuhlmann, T., Lingfeld, G., Bitsch, A., Schuchardt, J. & Brück, W. Acute axonal damage in multiple sclerosis is most extensive in early disease stages and decreases over time. *Brain* **125**, 2202–2212 (2002).
43. Choi, S. R. *et al.* Meningeal inflammation plays a role in the pathology of primary progressive multiple sclerosis. *Brain* **135**, 2925–2937 (2012).
44. Carbajal, K. S. *et al.* Th Cell Diversity in Experimental Autoimmune Encephalomyelitis and Multiple Sclerosis. *J. Immunol.* **195**, 2552–2559 (2015).
45. Allan, S. M. & Rothwell, N. J. Cytokines and acute neurodegeneration. *Nat. Rev. Neurosci.* **2**, 734–744 (2001).
46. Siffrin, V. *et al.* In Vivo Imaging of Partially Reversible Th17 Cell-Induced Neuronal Dysfunction in the Course of Encephalomyelitis. *Immunity* **33**, 424–436 (2010).
47. Aloisi, F. & Pujol-Borrell, R. Lymphoid neogenesis in chronic inflammatory diseases. *Nat. Rev. Immunol.* **6**, 205–217 (2006).
48. Bar-Or, A. *et al.* Abnormal B-cell cytokine responses a trigger of T-cell-mediated disease in MS? *Ann. Neurol.* **67**, 452–461 (2010).
49. Schluesener, H. J., Sobel, R. A., Linington, C. & Weiner, H. L. A monoclonal antibody against a myelin oligodendrocyte glycoprotein induces relapses and demyelination in central nervous system autoimmune disease. *J. Immunol.* **139**, 4016–21 (1987).
50. Vanguri, P. & Shin, M. L. Activation of Complement by Myelin: Identification of C1-Binding Proteins of Human Myelin from Central Nervous Tissue. *J. Neurochem.* **46**, 1535–1541 (1986).
51. Vanguri, P., Koski, C. L., Silverman, B. & Shin, M. L. Complement activation by

isolated myelin: Activation of the classical pathway in the absence of myelin-specific antibodies. *Proc. Natl. Acad. Sci. U. S. A.* **79**, 3290–3294 (1982).

52. Huizinga, R. *et al.* Immunization with neurofilament light protein induces spastic paresis and axonal degeneration in biozzi ABH mice. *J. Neuropathol. Exp. Neurol.* **66**, 295–304 (2007).
53. Mathey, E. K. *et al.* Neurofascin as a novel target for autoantibody-mediated axonal injury. *J. Exp. Med.* **204**, 2363–2372 (2007).
54. Levin, M. C. *et al.* Autoimmunity due to molecular mimicry as a cause of neurological disease. *Nat. Med.* **8**, 509–513 (2002).
55. Lee, S. *et al.* A potential link between autoimmunity and neurodegeneration in immune-mediated neurological disease. *J. Neuroimmunol.* **235**, 56–69 (2011).
56. JN, D. & LA, G. Antibodies to the RNA Binding Protein Heterogeneous Nuclear Ribonucleoprotein A1 Colocalize to Stress Granules Resulting in Altered RNA and Protein Levels in a Model of Neurodegeneration in Multiple Sclerosis. *J. Clin. Cell. Immunol.* **07**, (2016).
57. Silber, E., Semra, Y. K., Gregson, N. A. & Sharief, M. K. Patients with progressive multiple sclerosis have elevated antibodies to neurofilament subunit. *Neurology* **58**, 1372–1381 (2002).
58. Cléry, A. & Allain, F. H.-T. FROM STRUCTURE TO FUNCTION OF RNA BINDING DOMAINS. (2013).
59. Lenzken, S. C., Achsel, T., Carrì, M. T. & Barabino, S. M. L. Neuronal RNA-binding proteins in health and disease. *Wiley Interdiscip. Rev. RNA* **5**, 565–576 (2014).
60. Ratti, A. & Buratti, E. Physiological functions and pathobiology of TDP-43 and FUS/TLS proteins. *J. Neurochem.* **138 Suppl**, 95–111 (2016).
61. Thelen, M. P. & Kye, M. J. The Role of RNA Binding Proteins for Local mRNA Translation: Implications in Neurological Disorders. *Front. Mol. Biosci.* **6**, 161 (2019).
62. Fogel, B. L. *et al.* RBFOX1 regulates both splicing and transcriptional networks in human neuronal development. *Hum. Mol. Genet.* **21**, 4171–4186 (2012).
63. Zhang, C. *et al.* Integrative modeling defines the nova splicing-regulatory network

and its combinatorial controls. *Science (80-.).* **329**, 439–443 (2010).

64. Boutz, P. L. *et al.* A post-transcriptional regulatory switch in polypyrimidine tract-binding proteins reprograms alternative splicing in developing neurons. *Genes Dev.* **21**, 1636–1652 (2007).
65. Iijima, T. *et al.* SAM68 regulates neuronal activity-dependent alternative splicing of neurexin-1. *Cell* **147**, 1601–1614 (2011).
66. Ascano, M., Gerstberger, S. & Tuschl, T. Multi-disciplinary methods to define RNA-protein interactions and regulatory networks. *Curr. Opin. Genet. Dev.* **23**, 20–28 (2013).
67. Voronina, E., Seydoux, G., Sassone-Corsi, P. & Nagamori, I. RNA granules in germ cells. *Cold Spring Harb. Perspect. Biol.* **3**, (2011).
68. Hentze, M. W., Castello, A., Schwarzl, T. & Preiss, T. A brave new world of RNA-binding proteins. *Nat. Rev. Mol. Cell Biol.* **19**, 327–341 (2018).
69. Stoecklin, G. & Kedersha, N. Relationship of GW/P-bodies with stress granules. *Adv. Exp. Med. Biol.* **768**, 197–211 (2013).
70. Guo, Q., Shi, X. & Wang, X. RNA and liquid-liquid phase separation. *Non-coding RNA Res.* **6**, 92–99 (2021).
71. Maharana, S. *et al.* RNA buffers the phase separation behavior of prion-like RNA binding proteins. *Science (80-.).* **360**, 918–921 (2018).
72. Patel, A. *et al.* A Liquid-to-Solid Phase Transition of the ALS Protein FUS Accelerated by Disease Mutation. *Cell* **162**, 1066–1077 (2015).
73. Molliex, A. *et al.* Phase Separation by Low Complexity Domains Promotes Stress Granule Assembly and Drives Pathological Fibrillization. *Cell* **163**, 123–133 (2015).
74. Mateju, D. *et al.* An aberrant phase transition of stress granules triggered by misfolded protein and prevented by chaperone function. *EMBO J.* **36**, 1669–1687 (2017).
75. Dormann, D. *et al.* ALS-associated fused in sarcoma (FUS) mutations disrupt transportin-mediated nuclear import. *EMBO J.* **29**, 2841–2857 (2010).
76. Gami-Patel, P., Bandopadhyay, R., Brelstaff, J., Revesz, T. & Lashley, T. The presence of heterogeneous nuclear ribonucleoproteins in frontotemporal lobar

degeneration with FUS-positive inclusions. *Neurobiol. Aging* **46**, 192–203 (2016).
77. Belzil, V. V., Gendron, T. F. & Petrucelli, L. RNA-mediated toxicity in neurodegenerative disease. *Mol. Cell. Neurosci.* **56**, 406–419 (2013).
78. Libner, C. D., Salapa, H. E. & Levin, M. C. The potential contribution of dysfunctional RNA-binding proteins to the pathogenesis of neurodegeneration in multiple sclerosis and relevant models. *Int. J. Mol. Sci.* **21**, 1–16 (2020).
79. Ling, S. C., Polymenidou, M. & Cleveland, D. W. Converging mechanisms in als and FTD: Disrupted RNA and protein homeostasis. *Neuron* **79**, 416–438 (2013).
80. Cookson, M. R. RNA-binding proteins implicated in neurodegenerative diseases. *Wiley Interdiscip. Rev. RNA* **8**, (2017).
81. Ramaswami, M., Taylor, J. P. & Parker, R. XAltered ribostasis: RNA-protein granules in degenerative disorders. *Cell* **154**, (2013).
82. Polymenidou, M. *et al.* Long pre-mRNA depletion and RNA missplicing contribute to neuronal vulnerability from loss of TDP-43. *Nat. Neurosci.* **14**, 459–468 (2011).
83. Chia, R., Chiò, A. & Traynor, B. J. Novel genes associated with amyotrophic lateral sclerosis: diagnostic and clinical implications. *Lancet Neurol.* **17**, 94–102 (2018).
84. Sreedharan, J. *et al.* TDP-43 mutations in familial and sporadic amyotrophic lateral sclerosis. *Science (80-.).* **319**, 1668–1672 (2008).
85. Giordana, M. T. *et al.* TDP-43 redistribution is an early event in sporadic amyotrophic lateral sclerosis. *Brain Pathol.* **20**, 351–360 (2010).
86. Gerbino, V., Carrì, M. T., Cozzolino, M. & Achsel, T. Mislocalised FUS mutants stall spliceosomal snRNPs in the cytoplasm. *Neurobiol. Dis.* **55**, 120–128 (2013).
87. Yamazaki, T. *et al.* FUS-SMN Protein Interactions Link the Motor Neuron Diseases ALS and SMA. *Cell Rep.* **2**, 799–806 (2012).
88. Sharma, A. *et al.* ALS-associated mutant FUS induces selective motor neuron degeneration through toxic gain of function. *Nat. Commun.* **7**, (2016).
89. Mitra, J. *et al.* Motor neuron disease-associated loss of nuclear TDP-43 is linked to DNA double-strand break repair defects. *Proc. Natl. Acad. Sci.* **116**, 4696–4705 (2019).
90. Huang, W. *et al.* TDP-43: From Alzheimer's Disease to Limbic-Predominant Age-

Related TDP-43 Encephalopathy. *Front. Mol. Neurosci.* **0**, 26 (2020).

91. LaClair, K. D. *et al.* Depletion of TDP-43 decreases fibril and plaque β-amyloid and exacerbates neurodegeneration in an Alzheimer's mouse model. *Acta Neuropathol.* **132**, 859 (2016).
92. Masaki, K. *et al.* RNA-binding protein altered expression and mislocalization in MS. *Neurol. - Neuroimmunol. Neuroinflammation* **7**, 704 (2020).
93. Bekenstein, U. & Soreq, H. Heterogeneous nuclear ribonucleoprotein A1 in health and neurodegenerative disease: From structural insights to post-transcriptional regulatory roles. *Mol. Cell. Neurosci.* **56**, 436–446 (2013).
94. Jean-Philippe, J., Paz, S. & Caputi, M. hnRNP A1: The Swiss Army Knife of Gene Expression. *Int. J. Mol. Sci.* **14**, 18999 (2013).
95. Thibault, P. A. *et al.* hnRNP A/B Proteins: An Encyclopedic Assessment of Their Roles in Homeostasis and Disease. *Biol. 2021, Vol. 10, Page 712* **10**, 712 (2021).
96. Mayeda, A. & Krainer, A. R. Regulation of alternative pre-mRNA splicing by hnRNP A1 and splicing factor SF2. *Cell* **68**, 365–375 (1992).
97. Mayeda, A., Munroe, S. H., Cáceres, J. F. & Krainer, A. R. Function of conserved domains of hnRNP A1 and other hnRNP A/B proteins. *EMBO J.* **13**, 5483–5495 (1994).
98. Clarke, J. P., Thibault, P. A., Salapa, H. E. & Levin, M. C. A Comprehensive Analysis of the Role of hnRNP A1 Function and Dysfunction in the Pathogenesis of Neurodegenerative Disease. *Front. Mol. Biosci.* **0**, 217 (2021).
99. Geuens, T., Bouhy, D. & Timmerman, V. The hnRNP family: insights into their role in health and disease. *Hum. Genet.* **135**, 851 (2016).
100. Tavanez, J. P., Madl, T., Kooshapur, H., Sattler, M. & Valcárcel, J. HnRNP A1 Proofreads 3' Splice Site Recognition by U2AF. *Mol. Cell* **45**, 314–329 (2012).
101. Ding, J. *et al.* Crystal structure of the two-RRM domain of hnRNP A1 (UP1) complexed with single-stranded telomeric DNA. *Genes Dev.* **13**, 1102–1115 (1999).
102. Izaurralde, E. *et al.* A Role for the M9 Transport Signal of hnRNP A1 in mRNA Nuclear Export. *J. Cell Biol.* **137**, 27 (1997).
103. Clarke, J. P. W. E. *et al.* Multiple sclerosis-associated hnrnpa1 mutations alter

hnrnpa1 dynamics and influence stress granule formation. *Int. J. Mol. Sci.* **22**, 1–22 (2021).

104. Donev, R., Newall, A., Thome, J. & Sheer, D. A Role for SC35 and hnRNPA1 in the Determination of Amyloid Precursor Protein Isoforms. *Mol. Psychiatry* **12**, 681 (2007).
105. Kashima, T., Rao, N., David, C. J. & Manley, J. I. hnRNP A1 functions with specificity in repression of SMN2 exon 7 splicing. *Hum. Mol. Genet.* **16**, 3149–3159 (2007).
106. Levin, M., Lee, S., Shin, Y., Salapa, H. & Ketch, P. Novel Mechanism of Disease: Altered RNA metabolism due a dysfunctional RNA binding protein contributes to neurodegeneration in MS (P2.362). *Neurology* **88**, (2017).
107. Low, Y.-H., Asi, Y., Foti, S. C. & Lashley, T. Heterogeneous Nuclear Ribonucleoproteins: Implications in Neurological Diseases. *Mol. Neurobiol. 2020 582* **58**, 631–646 (2020).
108. Salapa, H. E., Libner, C. D. & Levin, M. C. Dysfunctional RNA-binding protein biology and neurodegeneration in experimental autoimmune encephalomyelitis in female mice. *J. Neurosci. Res.* **98**, 704–717 (2020).
109. Salapa, H. E., Hutchinson, C., Popescu, B. F. & Levin, M. C. Neuronal RNA-binding protein dysfunction in multiple sclerosis cortex. *Ann. Clin. Transl. Neurol.* **7**, 1214–1224 (2020).
110. Salapa, H. E., Johnson, C., Hutchinson, C., Popescu, B. F. & Levin, M. C. Dysfunctional RNA binding proteins and stress granules in multiple sclerosis. *J. Neuroimmunol.* **324**, 149–156 (2018).
111. Berson, A. *et al.* Cholinergic-associated loss of hnRNP-A/B in Alzheimer's disease impairs cortical splicing and cognitive function in mice. *EMBO Mol. Med.* **4**, 730–742 (2012).
112. Honda, H. *et al.* Loss of hnRNPA1 in ALS spinal cord motor neurons with TDP-43-positive inclusions. *Neuropathology* **35**, 37–43 (2015).
113. S, J. *et al.* ATPase-Modulated Stress Granules Contain a Diverse Proteome and Substructure. *Cell* **164**, 487–498 (2016).
114. Mazroui, R. *et al.* Inhibition of ribosome recruitment induces stress granule

formation independently of eukaryotic initiation factor 2α phosphorylation. *Mol. Biol. Cell* **17**, 4212–4219 (2006).

115. Campos-Melo, D., Hawley, Z. C. E., Droppelmann, C. A. & Strong, M. J. The Integral Role of RNA in Stress Granule Formation and Function. *Front. Cell Dev. Biol.* **9**, 808 (2021).
116. Anderson, P. & Kedersha, N. Stress granules: the Tao of RNA triage. *Trends Biochem. Sci.* **33**, 141–150 (2008).
117. Guil, S., Long, J. C. & Cáceres, J. F. hnRNP A1 Relocalization to the Stress Granules Reflects a Role in the Stress Response. *Mol. Cell. Biol.* **26**, 5744–5758 (2006).
118. Vanderweyde, T., Youmans, K., Liu-Yesucevitz, L. & Wolozin, B. Role of stress granules and RNA-binding proteins in neurodegeneration: A mini-review. *Gerontology* **59**, 524–533 (2013).
119. Baradaran-Heravi, Y., Van Broeckhoven, C. & van der Zee, J. Stress granule mediated protein aggregation and underlying gene defects in the FTD-ALS spectrum. *Neurobiol. Dis.* **134**, (2020).
120. Ash, P. E. A., Vanderweyde, T. E., Youmans, K. L., Apicco, D. J. & Wolozin, B. Pathological stress granules in Alzheimer's disease. *Brain Res.* **1584**, 52–58 (2014).
121. Zhang, Y. J. *et al.* Poly(GR) impairs protein translation and stress granule dynamics in C9orf72-associated frontotemporal dementia and amyotrophic lateral sclerosis. *Nat. Med.* **24**, 1136–1142 (2018).
122. Zhang, P. *et al.* Chronic optogenetic induction of stress granules is cytotoxic and reveals the evolution of ALS-FTD pathology. *Elife* **8**, (2019).
123. Gendron, T. F., Rademakers, R. & Petrucelli, L. TARDBP mutation analysis in TDP-43 proteinopathies and deciphering the toxicity of mutant TDP-43. *J. Alzheimer's Dis.* **33**, (2013).
124. Orrù, S. *et al.* Reduced stress granule formation and cell death in fibroblasts with the A382T mutation of TARDBP gene: Evidence for loss of TDP-43 nuclear function. *Hum. Mol. Genet.* **25**, 4473–4483 (2016).
125. Klebe, R. J. & Ruddle, R. H. Neuroblastoma: Cell culture analysis of a

differentiating stem cell system - Google Acadêmico. *Jounal Cell Biol.* **43**, A69 (1969).

126. Tremblay, R. G. *et al.* Differentiation of mouse Neuro 2A cells into dopamine neurons. *J. Neurosci. Methods* **186**, 60–67 (2010).
127. Olmsted, J. B., Carlson, K., Klebe, R., Ruddle, F. & Rosenbaum, J. Isolation of microtubule protein from cultured mouse neuroblastoma cells. *Proc. Natl. Acad. Sci. U. S. A.* **65**, 129–136 (1970).
128. Evangelopoulos, M. E., Weis, J. & Krüttgen, A. Signalling pathways leading to neuroblastoma differentiation after serum withdrawal: HDL blocks neuroblastoma differentiation by inhibition of EGFR. *Oncogene* **24**, 3309–3318 (2005).
129. Iguchi, Y. *et al.* TDP-43 depletion induces neuronal cell damage through dysregulation of Rho family GTPases. *J. Biol. Chem.* **284**, 22059–22066 (2009).
130. Iguchi, Y. *et al.* Exosome secretion is a key pathway for clearance of pathological TDP-43. *Brain* **139**, 3187–3201 (2016).
131. Winton, M. J. *et al.* Disturbance of nuclear and cytoplasmic TAR DNA-binding protein (TDP-43) induces disease-like redistribution, sequestration, and aggregate formation. *J. Biol. Chem.* **283**, 13302–13309 (2008).
132. Hornburg, D. *et al.* Deep proteomic evaluation of primary and cell line motoneuron disease models delineates major differences in neuronal characteristics. *Mol. Cell. Proteomics* **13**, 3410–3420 (2014).
133. Wheeler, J. R., Matheny, T., Jain, S., Abrisch, R. & Parker, R. Distinct stages in stress granule assembly and disassembly. *Elife* **5**, (2016).
134. Chen, S., Zhou, Y., Chen, Y. & Gu, J. fastp: an ultra-fast all-in-one FASTQ preprocessor. *Bioinformatics* **34**, i884–i890 (2018).
135. Schneider, V. & Church, D. Genome reference consortium. *The NCBI Handbook* 117 https://www.ncbi.nlm.nih.gov/grc/human (2013).
136. Dobin, A. *et al.* STAR: ultrafast universal RNA-seq aligner. *Bioinformatics* **29**, 15–21 (2013).
137. Anders, S., Pyl, P. T. & Huber, W. HTSeq—a Python framework to work with high-throughput sequencing data. *Bioinformatics* **31**, 166–169 (2015).
138. Love, M. I., Huber, W. & Anders, S. Moderated estimation of fold change and

dispersion for RNA-seq data with DESeq2. *Genome Biol. 2014 1512* **15**, 1–21 (2014).

139. Wilson, A. & Norden, N. The R Project for Statistical Computing The R Project for Statistical Computing. *URL: http://www. r-project. org/254* vol. 3 1–9 https://www.r-project.org/ (2015).
140. Shannon, P. *et al.* Cytoscape: A software Environment for integrated models of biomolecular interaction networks. *Genome Res.* **13**, 2498–2504 (2003).
141. Szklarczyk, D. *et al.* The STRING database in 2021: Customizable protein-protein networks, and functional characterization of user-uploaded gene/measurement sets. *Nucleic Acids Res.* **49**, D605–D612 (2021).
142. Yang, Y.-C. T. *et al.* CLIPdb: a CLIP-seq database for protein-RNA interactions. *BMC Genomics 2015 161* **16**, 1–8 (2015).
143. Howe, K. L. *et al.* Ensembl 2021. *Nucleic Acids Res.* **49**, D884–D891 (2021).
144. Meijering, E. *et al.* Design and Validation of a Tool for Neurite Tracing and Analysis in Fluorescence Microscopy Images. *Cytom. Part A* **58**, 167–176 (2004).
145. You, Q. *et al.* Role of miR-124 in the regulation of retinoic acid-induced Neuro-2A cell differentiation. *Neural Regen. Res.* **15**, 1133–1139 (2020).
146. Han, H. RNA interference to knock down gene expression. *Methods Mol. Biol.* **1706**, 293–302 (2018).
147. Hancock, M. K., Kopp, L., Kaur, N. & Hanson, B. J. A Facile Method for Simultaneously Measuring Neuronal Cell Viability and Neurite Outgrowth. *Curr. Chem. Genomics Transl. Med.* **9**, 6–16 (2015).
148. Purice, M. D. & Taylor, J. P. Linking hnRNP function to ALS and FTD pathology. *Front. Neurosci.* **12**, (2018).
149. Steinacker, P., Barschke, P. & Otto, M. Biomarkers for diseases with TDP-43 pathology. *Mol. Cell. Neurosci.* **97**, 43–59 (2019).
150. Hanson, K. A., Kim, S. H. & Tibbetts, R. S. RNA-Binding Proteins in Neurodegenerative Disease: TDP-43 and Beyond. *Wiley Interdiscip. Rev. RNA* **3**, 265 (2012).
151. Harley, J., Clarke, B. E. & Patani, R. The Interplay of RNA Binding Proteins, Oxidative Stress and Mitochondrial Dysfunction in ALS. *Antioxidants* **10**, (2021).

152. Arnold, E. S. *et al.* ALS-linked TDP-43 mutations produce aberrant RNA splicing and adult-onset motor neuron disease without aggregation or loss of nuclear TDP-43. *Proc. Natl. Acad. Sci. U. S. A.* **110**, (2013).
153. Igaz, L. M. *et al.* Dysregulation of the ALS-associated gene TDP-43 leads to neuronal death and degeneration in mice. *J. Clin. Invest.* **121**, 726–738 (2011).
154. Dana, H. *et al.* Molecular Mechanisms and Biological Functions of siRNA. *Int. J. Biomed. Sci.* **13**, 48–57 (2017).
155. Sariyer, I. K. Transfection of neuronal cultures. *Methods Mol. Biol.* **1078**, 133–139 (2013).
156. Nishimura, A. L. *et al.* Allele-specific knockdown of ALS-associated mutant TDP-43 in neural stem cells derived from induced pluripotent stem cells. *PLoS One* **9**, (2014).
157. Fiesel, F. C. *et al.* Knockdown of transactive response DNA-binding protein (TDP-43) downregulates histone deacetylase 6. *EMBO J.* **29**, 209–221 (2010).
158. Fiesel, F. C., Schurr, C., Weber, S. S. & Kahle, P. J. TDP-43 knockdown impairs neurite outgrowth dependent on its target histone deacetylase 6. *Mol. Neurodegener. 2011 61* **6**, 1–10 (2011).
159. Ling, S. C. Synaptic paths to neurodegeneration: The emerging role of TDP-43 and FUS in synaptic functions. *Neural Plast.* **2018**, (2018).
160. Deshaies, J. E. *et al.* TDP-43 regulates the alternative splicing of hnRNP A1 to yield an aggregation-prone variant in amyotrophic lateral sclerosis. *Brain* **141**, 1320–1333 (2018).
161. Paramasivam, M. *et al.* Protein hnRNP A1 and its derivative Up1 unfold quadruplex DNA in the human KRAS promoter: Implications for transcription. *Nucleic Acids Res.* **37**, 2841–2853 (2009).
162. Hay, D. C., Kemp, G. D., Dargemont, C. & Hay, R. T. Interaction between hnRNPA1 and IκBα Is Required for Maximal Activation of NF-κB-Dependent Transcription. *Mol. Cell. Biol.* **21**, 3482 (2001).
163. Sahu, I., Sangith, N., Ramteke, M., Gadre, R. & Venkatraman, P. A novel role for the proteasomal chaperone PSMD9 and hnRNPA1 in enhancing IκBα degradation and NF-κB activation - Functional relevance of predicted PDZ

domain-motif interaction. *FEBS J.* **281**, 2688–2709 (2014).

164. Hayden, M. S. & Ghosh, S. Shared Principles in NF-κB Signaling. *Cell* **132**, 344–362 (2008).
165. Zahler, A. M., Damgaard, C. K., Kjems, J. & Caputi, M. SC35 and Heterogeneous Nuclear Ribonucleoprotein A/B Proteins Bind to a Juxtaposed Exonic Splicing Enhancer/Exonic Splicing Silencer Element to Regulate HIV-1 tat Exon 2 Splicing. *J. Biol. Chem.* **279**, 10077–10084 (2004).
166. Liu, T.-Y. *et al.* Muscle developmental defects in heterogeneous nuclear Ribonucleoprotein A1 knockout mice. *Open Biol.* **7**, (2017).
167. Protter, D. S. W. & Parker, R. Principles and Properties of Stress Granules. *Trends Cell Biol.* **26**, 668–679 (2016).